NASA Technical Paper 3036

August 1990

Effect of Tail Size Reductions on Longitudinal Aerodynamic Characteristics of a Three-Surface F-15 Model With Nonaxisymmetric Nozzles

Mark C. Frassinelli
and George T. Carson, Jr.

NASA

NASA Technical Paper 3036

1990

Effect of Tail Size Reductions on Longitudinal Aerodynamic Characteristics of a Three-Surface F-15 Model With Nonaxisymmetric Nozzles

Mark C. Frassinelli
Air Force Wright Research and Development Center
Wright-Patterson Air Force Base, Ohio

George T. Carson, Jr.
Langley Research Center
Hampton, Virginia

National Aeronautics and Space Administration
Office of Management
Scientific and Technical Information Division

Summary

An investigation was conducted in the Langley 16-Foot Transonic Tunnel to determine the effects of horizontal- and vertical-tail size reductions on the longitudinal aerodynamic characteristics of a modified F-15 model with canards and two-dimensional, convergent-divergent nozzles. This study focused primarily on quantifying the drag decrease at low angles of attack produced by tail size reductions. The model was tested at Mach numbers of 0.40, 0.90, and 1.20 over an angle-of-attack range from $-2°$ to $10°$. The nozzle exhaust flow was simulated by using high-pressure air at nozzle pressure ratios from 1.0 (jet off) to 7.5. Data were obtained on the baseline configuration with and without tails and with reduced horizontal- and/or vertical-tail sizes that were 75, 50, and 25 percent of the baseline tail areas. Results of this investigation indicated that the reduction or removal of tail surfaces produced significant decreases in total drag. Tail size reductions had a favorable effect on the afterbody-tail-nozzle flow field that generated substantial decreases in tail interference drag, particularly at transonic speeds. The elimination of all tails produced the largest total drag reduction, and the removal of the vertical tails alone generated the second largest drag reduction at transonic and supersonic speeds. The removal of the vertical tails was much more effective at reducing drag than the removal of the horizontal tails. Over the entire speed range, the 25-percent horizontal- and vertical-tail combination was the most effective at reducing drag other than with all tails removed. As expected, decreases in horizontal-tail size generated reduced longitudinal stability. Reductions in vertical-tail size generated no significant effects on longitudinal stability and produced a small afterbody lift increase.

Introduction

The future air combat arena will require fighter aircraft with improved performance in several flight regimes. These aircraft will probably be designed with sustained supersonic cruise, high-angle-of-attack maneuverability and agility, and short takeoff and landing capabilities to operate from bomb-damaged airfields (ref. 1). Several studies have shown the significant air combat advantages of performing transient maneuvers at high angles of attack, including brief excursions into post-stall conditions (refs. 1 to 3). However, the flight envelope of current aircraft is limited because of the degraded longitudinal, lateral, and directional stability and control at high angles of attack. This degradation is a result of adverse flow conditions that result in a severe loss in the effectiveness of conventional aerodynamic control surfaces. Providing improved aerodynamics and increased control effectiveness will allow rapid, precise maneuvering in a greatly expanded flight envelope.

One promising method of providing control forces and moments that is not dependent on angle of attack and dynamic pressure (as are aerodynamic controls) is the vectoring of the engine exhaust. Studies have shown that pitch- and yaw-vectoring nozzles can provide large improvements in pitch rate, yaw rate, and maximum controllable angle of attack. Thrust vectoring significantly expands the low-speed, high-angle-of-attack flight envelope by providing enhanced aircraft agility in the near-stall and post-stall angle-of-attack ranges (refs. 4 to 7). These nozzles can also be designed with thrust reversers to provide rapid decelerations to corner velocity and force overshoots by an adversary. Thrust vectoring may also allow aircraft designers to reduce or eliminate conventional aerodynamic control surfaces. Conventional aerodynamic control surfaces are usually sized for low-speed operations and provide more control power than required at high speeds. Since propulsive control effectiveness increases at low speeds, aerodynamic control surfaces such as the horizontal and vertical tails can be significantly reduced or even eliminated. Thus, thrust vectoring can allow the development of aircraft that are optimized for high supersonic cruise efficiency but also possess enhanced low-speed, high-angle-of-attack agility (refs. 4, 8, and 9).

Reduction or elimination of tail surfaces provides significant drag and weight savings. Tail removal can greatly reduce the afterbody (aft 25 to 35 percent of aircraft length) drag (35 to 50 percent of total aircraft drag) of a typical fighter. Experimental studies have indicated that the total drag of a typical twin-engine fighter can be reduced 12 to 38 percent by the removal of tail surfaces (refs. 10 to 14). Further drag reduction can be generated through redesign of the afterbody and removal of tail attachment hardware.

This investigation was conducted to determine the longitudinal aerodynamic effects of horizontal- and/or vertical-tail size reductions at low angles of attack. This study focused primarily on quantifying the drag decrease from tail size reductions. Experiments were conducted in the Langley 16-Foot Transonic Tunnel on a model of the the experimental F-15 Short Takeoff and Landing Maneuver Technology Demonstrator (S/MTD) (ref. 15). This configuration utilizes canards and two-dimensional thrust-vectoring nozzles for enhanced maneuverability. The baseline tails and several reduced horizontal- and vertical-tail sizes were tested in various combinations at Mach numbers of 0.40, 0.90, and 1.20 up to $10°$ angle of attack. To provide data for

follow-on flight-test plans, all data were obtained with the nonaxisymmetric nozzles rotated 90° to allow yaw thrust vectoring. This report also presents the effects of reduced tail sizes on total drag and the skin-friction, interference, and wave-drag components.

Symbols and Abbreviations

All longitudinal forces and moments are referenced to the stability axis system. The model moment reference center was near the $\bar{c}/4$ location of the wing at fuselage station 36.741 and waterline 0.908.

A_{ex}	nozzle exit area, 6.60 in^2
A_{fus}	maximum cross-sectional area of model fuselage enclosed by metric-break seal at nozzle connect station, in^2
$A_{\text{seal,aft}}$	internal cross-sectional area enclosed by metric-break seal at nozzle connect station, in^2
$A_{\text{seal,for}}$	area enclosed by metric-break seal between strut support and model shell, in^2
A_{th}	nozzle throat area, 5.20 in^2
b	wing span, 42.80 in.
b_t	tail span, in.
C_D	total aircraft drag coefficient, Drag/$q_\infty S$ (eq. (3))
$C_{D,\text{aen}}$	drag coefficient of aircraft except nozzles
$C_{D,\text{NOZ}}$	total drag coefficient of two nozzles, Nozzle drag/$q_\infty S$ (eq. (2))
$C_{D,\text{NOZ}(pr)}$	nozzle integrated pressure drag coefficient
$C_{D,\text{NOZ}(sf)}$	nozzle skin-friction drag coefficient
$C_{D,t(sf)}$	tail skin-friction drag coefficient
$C_{D,t(w)}$	tail wave-drag coefficient
$\Delta C_{D,it}$	increment in total tail interference-drag coefficient (eq. (4))
$\Delta C_{D,it(\text{aen})}$	tail interference-drag increment on aircraft except nozzles (eq. (6))
$\Delta C_{D,it(\text{noz})}$	tail interference-drag increment on nozzles (eq. (5))
C_L	total aircraft lift coefficient, Lift/$q_\infty S$
$C_{L,\text{NOZ}}$	total lift coefficient of two nozzles, Nozzle lift/$q_\infty S$
C_m	total aircraft pitching-moment coefficient, Pitching moment/$q_\infty S\bar{c}$
$C_{m,0}$	zero-lift pitching-moment coefficient
$\bar{c}$	mean geometric chord, 15.942 in.
c_R	tail root chord, in.
c_T	tail tip chord, in.
D_{aen}	drag on aircraft except nozzles, lbf (eq. (1))
D_{bal}	balance measured drag on aircraft except nozzles, lbf
M	free-stream Mach number
p_{es}	local static pressure external to metric-break seal, psi
p_{in}	local internal static pressure, psi
$p_{t,j}$	jet total pressure, psi
p_∞	free-stream static pressure, psi
q_∞	free-stream dynamic pressure, psi
S	wing reference area, 608.0 in^2
s	horizontal-tail slot length, in.
α	angle of attack, deg
δ_c	canard deflection angle (positive with leading edge up), deg
δ_{ht}	horizontal-tail deflection angle (positive with leading edge up), deg
δ_r	rudder deflection angle (positive with trailing edge left looking upstream), deg
$\delta_{v,y}$	nozzle geometric yaw-vector angle (positive with trailing edge left looking upstream), deg
ϵ	nozzle expansion ratio, A_{ex}/A_{th}
η_D	drag reduction efficiency, $\frac{C_D \text{ reduction relative to baseline}}{\text{Maximum } C_D \text{ reduction (tails-off)}}$

Abbreviations:

A/B	afterburning
aero.	aerodynamic
BL	buttock line, in.
config.	configuration

FS	fuselage station, in.
HT	horizontal tail
LE	leading edge
NACA	National Advisory Committee for Aeronautics
NPR	nozzle pressure ratio, $p_{t,j}/p_\infty$
S/MTD	Short Takeoff and Landing Maneuver Technology Demonstrator
VT	vertical tail
WL	waterline, in.
2-D C-D	two-dimensional convergent-divergent

Apparatus and Procedure

Wind Tunnel

This investigation was conducted in the Langley 16-Foot Transonic Tunnel. The facility is a closed-circuit, single-return, continuous-flow, atmospheric wind tunnel with a slotted, octagonal test section. The test-section airspeed is variable between Mach 0.20 and 1.30. Speeds up to Mach 1.05 are obtained with tunnel main drive fans and speeds from Mach 1.05 to 1.30 are obtained with a combination of main-drive and test-section plenum suction provided by a compressor. Further details on dimensions and operating characteristics of the Langley 16-Foot Transonic Tunnel are in reference 16.

Model

Tests were conducted on a 1/12th (8.33-percent) scale model of the experimental F-15 Short Takeoff and Landing Maneuver Technology Demonstrator (S/MTD), which uses canards and thrust-vectoring nozzles for increased maneuverability. A sketch of the model is shown in figure 1 and the model geometry is presented in table 1. The model is a partially metric jet-effects model with faired-over inlets and a propulsion simulation system. Forces and moments on the metric portions of the model, which include the wing, fuselage, and tails, were measured by an internal balance. The nonmetric nozzles (which were not on the balance) were instrumented with static-pressure orifices to obtain nozzle forces and moments. Since the nozzles are nonmetric, the thrust forces and moments generated by the jet exhaust flow were not measured. However, the jet-induced effects on the aircraft external aerodynamic characteristics were obtained. Figure 2 is a photograph of the model installed in the Langley 16-Foot Transonic Tunnel. The model was supported by a sting-strut support system through which high-pressure air lines and all instrumentation were routed. A high-pressure air system supplied a continuous flow of clean, dry air at a controlled temperature of approximately 550°R. High-pressure air was directed through the strut to a common air plenum and divided into airflow ducts for each of the two-dimensional convergent-divergent nozzles. Figure 3 shows the nonmetric twin-engine, propulsion-simulation support system. The metric break between the metric wing-fuselage-afterbody and the nonmetric nozzles was located at FS 52.727 as shown in figure 1. A flexible strip, inserted into slots machined into the metric portions of the model, was used as a seal at the metric-break station to inhibit flow through the gap between the nozzles and the afterbody. A flexible rubber seal was also located in the gap on the underside of the model, where the strut support attaches to the internal propulsion system hardware.

Horizontal and Vertical Tails

Data were obtained on the baseline configuration with and without tails as well as with reduced horizontal- and/or vertical-tail sizes that were 75, 50, and 25 percent of the baseline tail areas. Throughout this paper, the baseline-tail case refers to the 100-percent tail size and 0 percent refers to the tails-off case. Figures 4 and 5 show the dimensions of the horizontal and vertical tails. To eliminate any variation in tail-generated moments due to different tail distances from the reference center, the $\bar{c}/4$ location of each tail size was fixed at a constant model fuselage station. The vertical-tail $\bar{c}/4$ was at FS 54.335, and the horizontal-tail $\bar{c}/4$ was at FS 56.692. Figures 6, 7, and 8 are photographs of some of the horizontal- and vertical-tail combinations tested during this study.

Two-Dimensional Convergent-Divergent Nozzles

The two-dimensional convergent-divergent (2-D C-D) nozzle design used for this study simulates a variable-area internal expansion nozzle with a rectangular cross section. The throat area and exit area of the full-scale hardware can be varied by independent actuation of the convergent and divergent nozzle flaps. Figure 9 is a photograph of the nozzles mounted on the model. The nozzles in this investigation were rotated 90° relative to the nominal F-15 S/MTD pitch-vectoring nozzles. By deflecting the nozzle divergent flaps, the jet exhaust flow can be turned in the yaw plane. The nozzle internal geometry represents a nozzle optimized for afterburning operation up to low supersonic speeds. The design

nozzle pressure ratio of these nozzles was 4.40. Figure 10 shows the geometric characteristics of the nozzles at 0° yaw-vector angle. All data presented in this paper were obtained at a yaw-vector angle of 0°.

Instrumentation

Model forces and moments, excluding the nozzles, were measured by an internal six-component strain-gage balance. External nozzle forces and moments were determined through the integration of 168 external static-pressure orifices located on the pair of exhaust nozzles. The orifices were distributed on the nozzle external surface to ensure that anticipated variations in pressure coefficient would be measured. However, even with the large number of orifices used here, some details of the complex nozzle flow field may have been missed as a result of improper static-pressure tap locations. Internal-cavity pressures were measured at two locations near the flexible seal forward of the balance and at four locations near the seal at the nozzle connect station. Eighteen static pressures were also measured in the nozzle-afterbody metric-break gap on the external side of the flexible seal. Together, these internal-cavity and metric-seal pressures were used to make pressure-area tare corrections to the balance measurements. Jet total pressures and temperatures were measured in the flow duct upstream of each nozzle throat by five total-pressure probes and a thermocouple. All pressures were measured by individual pressure transducers except for the nozzle external pressures and nozzle metric-break pressures. These measurements were obtained by six internally mounted 32-port multiducers that were electronically scanned to simultaneously record the pressure on each of the 32 channels. The instruments were located in the model-forebody area and were continually compared with independent check pressures and recalibrated as necessary. Model attitude was determined by an accelerometer mounted in the model nose.

Tests

Data were taken at Mach numbers of 0.40, 0.90, and 1.20 and at angles of attack from $-2°$ up to 10° in 2° increments. Nozzle pressure ratio (NPR) was varied from 1.0 (jet off) to approximately 7.5. Angle-of-attack sweeps were conducted at scheduled nozzle pressure ratios representative of current turbofan operating conditions. Data were taken at NPR $\approx$ 3.8 for Mach 0.40, NPR $\approx$ 5.7 for Mach 0.90, and NPR $\approx$ 7.5 for Mach 1.20. Nozzle-pressure-ratio sweeps were conducted for selected configurations at 0° angle of attack. Table 2 provides a summary of the configurations and the conditions of data acquisition. The average Reynolds number, based on the wing mean aerodynamic chord, varied from approximately 3.3×10^6 at Mach 0.40 to approximately 5.1×10^6 at Mach 0.90 and approximately 5.4×10^6 at Mach 1.20. Boundary-layer transition was fixed on the model by means of 0.060-in-wide strips of No. 120 carborundum grit (refs. 17 and 18). These strips were located 0.80 in. aft (streamwise) of the nose and inlet fairings. Transition strips were also located on the wing, canards, horizontal tails, and vertical tails at 6 percent of the local chord.

Data Reduction

Data for the model and the wind tunnel were recorded simultaneously on magnetic tape. At each data point, 50 frames of data, taken at a rate of 10 frames per second, were used to obtain averaged recorded data. The averaged data were used to compute standard force and moment coefficients. All longitudinal force and moment data in this paper are referenced to the stability axis system, which passes through the moment reference center (fig. 1). Model angle of attack was corrected for flow angularity by applying an adjustment of 0.10°, which is the average upflow angle measured in the Langley 16-Foot Transonic Tunnel (ref. 16). Forces and moments on the entire model, except the nozzles, were measured by an internal six-component strain-gage balance. Balance force measurements were initially corrected for model weight tares and balance interactions. Corrections were also made to the balance data to account for internal-cavity and seal pressure-area tares.

The total drag on the aircraft except nozzles was computed by the following equation:

$$D_{\text{aen}} = D_{\text{bal}} + \sum(p_{es} - \rho_\infty)(A_{\text{fus}} - A_{\text{seal,aft}}) + \sum(p_{in} - p_\infty)A_{\text{seal,aft}} - \sum(p_{in} - p_\infty)A_{\text{seal,for}} \quad (1)$$

The corrected balance forces and moments were converted to coefficients based on the model wing reference area, span, and mean aerodynamic chord.

The forces and moments of the exhaust nozzles were obtained by integrating pressure measurements with the assigned projected areas and moment arms of each pressure orifice. The skin-friction drags of the nozzles and tails were computed using the method of Frankl and Voishel (refs. 19 and 20) for compressible turbulent flow on a flat plate. The total nozzle drag coefficient was obtained by adding the nozzle skin-friction drag to the pressure integrated nozzle drag as follows:

$$C_{D,\text{NOZ}} = C_{D,\text{NOZ}(pr)} + C_{D,\text{NOZ}(sf)} \quad (2)$$

Total aircraft drag coefficient was calculated by adding the drag on the aircraft except nozzles (as indicated by corrected balance data) to the nozzle drag as follows:

$$C_D = C_{D,\mathrm{NOZ}} + C_{D,\mathrm{aen}} \tag{3}$$

The interference-drag increment of the tails on the entire aircraft was determined for each tail combination relative to the baseline (100-percent horizontal and vertical tails) configuration. The tail interference-drag increment for the entire aircraft was determined from

$$\begin{aligned}\Delta C_{D,it} = {} & \left(C_{D\,(\mathrm{baseline})} - C_{D\,(\%\mathrm{HT}/\%\mathrm{VT})}\right) \\ & - \left(C_{D,t\,(sf)\,(\mathrm{baseline})} - C_{D,t\,(sf)\,(\%\mathrm{HT}/\%\mathrm{VT})}\right) \\ & - \left(C_{D,t\,(w)\,(\mathrm{baseline})} - C_{D,t\,(w)\,(\%\mathrm{HT}/\%\mathrm{VT})}\right)\end{aligned} \tag{4}$$

where $C_{D(\mathrm{baseline})}$ is the total aircraft drag coefficient for the baseline configuration as described previously, and $C_{D(\%\mathrm{HT}/\%\mathrm{VT})}$ is the total drag for each reduced tail size combination. The skin-friction drag plus form drag of each tail combination is included in $C_{D,t(sf)}$. At supersonic speeds, the interference-drag increment also includes the wave-drag coefficient of the tails ($C_{D,t(w)}$) as calculated by using the slender-body, equivalent-area theory described in reference 21.

The tail interference-drag increment is the combined effect of the tails on the nozzles and the remainder of the aircraft. The tail interference-drag increment on the nozzles alone was obtained by subtracting the nozzle drag of each tail configuration from the nozzle drag of the baseline configuration as follows:

$$\Delta C_{D,it(\mathrm{noz})} = C_{D,\mathrm{NOZ}(\mathrm{baseline})} - C_{D,\mathrm{NOZ}(\%\mathrm{HT}/\%\mathrm{VT})} \tag{5}$$

Nozzle drag is computed by integrating the pressure distribution over the nozzle external surface. Thus, this tail interference increment is the change in nozzle pressure distribution that results from the reduction in horizontal- and vertical-tail size.

The tail interference effects on the aircraft fuselage alone were determined by subtracting the tail interference-drag increment of the nozzles from the tail interference-drag increment of the total aircraft, or

$$\Delta C_{D,it(\mathrm{aen})} = \Delta C_{D,it} - \Delta_{D,it(\mathrm{noz})} \tag{6}$$

This interference term includes the effects of each tail surface on the fuselage and of the tail surfaces on each other as well as the effects of the afterbody and other parts of the aircraft on the tails. To avoid errors associated with the computation of lift-induced drag on the horizontal tails, wing, fuselage, and nozzles, these interference terms were computed only at 0° angle of attack.

Results and Discussion

The results of this investigation are presented in plotted coefficient format, and bar charts of drag comparisons at 0° angle of attack are included. The baseline configuration refers to the standard F-15 S/MTD with −5° canards, 0° nozzle flap deflection, 0° sideslip, and 100-percent (full-size) vertical and horizontal tails installed in the undeflected position unless otherwise specified.

Basic Data Comparisons

Nozzle pressure ratio effects. The effects of nozzle pressure ratio (NPR) on the longitudinal aerodynamic characteristics are shown in figure 11 for the baseline (100-percent tails) case and with the tails removed. At all test speeds, lift and pitching-moment characteristics for each configuration were generally independent of nozzle pressure ratio. However, drag coefficient varied as nozzle pressure ratio increased from jet off (NPR = 1) to the maximum test NPR. At Mach 0.40 (fig. 11(a)), increases in nozzle pressure ratio produced a small drag increase for the baseline configuration. This result may be caused by the jet entrainment effects of the overexpanded jet flow at an NPR below the design NPR (approximately 4.4) for this afterburning nozzle. The presence of tails adversely influenced the afterbody flow field to produce a jet-induced drag increment that was not present for the tails-off case. Without tails, variation in nozzle pressure ratio had no significant effect on total drag at $M = 0.40$. The drag trend was similar at Mach 0.90 and 1.20; however, little or no drag increase was generated as NPR approached design conditions. At underexpanded conditions (above design NPR), jet exhaust-flow simulation generated favorable afterbody-tail-nozzle flow interactions that reduced drag. This effect was probably the result of compression at the nozzle exit created by the increased diameter of the exhaust-flow plume.

As figure 12 indicates, the effect of NPR on nozzle drag followed the same trends as total aircraft drag discussed previously. At Mach 0.40, adverse afterbody-nozzle-jet interactions produced a small jet-induced drag increase at overexpanded conditions. At Mach 0.90 and 1.20, favorable interactions reduced nozzle drag relative to jet-off conditions, particularly at overexpanded conditions. These trends

are typical for jet-powered models and were obtained for both total drag and nozzle drag (ref. 14).

The results shown in figures 11 and 12 also highlight the relative insensitivity of aerodynamic characteristics to small differences in NPR. As shown subsequently, some data comparisons were made at NPR settings that were somewhat inconsistent. These inconsistencies were due to the removal (after the tests were complete) of known bad pressure measurements from the average jet total-pressure calculation used to compute NPR. Figure 11 shows the typical variation in NPR during this investigation. However, as figures 11 and 12 indicate, the effects of these small NPR variations on aerodynamic characteristics were very small. Thus, small differences in NPR values in various data comparisons had no significant effect on results presented herein.

Combined horizontal- and vertical-tail size reductions. The effects of reducing both the horizontal- and vertical-tail size on longitudinal aerodynamic characteristics at low angles of attack are presented in figure 13. At all test Mach numbers, a significant decrease in drag coefficient resulted from tail size reductions from 100 percent (full size) to 0 percent (tail off). Total aircraft drag increased with Mach number, but the drag-reduction increment due to tail size also increased at higher speeds. As figure 13(a) indicates at Mach 0.40, removal of the tails produced a drag decrease of approximately 0.0040 at 0° angle of attack. At higher angles of attack, the drag reduction was less. Almost half the drag decrease at $\alpha = 0°$ was generated by reducing tail size from 100 percent to 75 percent. Tail size reductions from 75 percent to 50 percent also generated a considerable drag coefficient decrease; however, further tail size reductions to 25 percent and 0 percent did not yield significant drag reductions. Thus, the relationship between tail size and drag was not linear at Mach 0.40. As expected, the drag reduction due to reduced tail size was not a function of surface area alone, but a combination of nozzle, afterbody, tail, and jet exhaust interactions.

At Mach 0.90, figure 13(b) shows similar drag decreases as both vertical- and horizontal-tail sizes were reduced. Half the drag decrease from removing all tails at 0° angle of attack was generated by the reduction from 100-percent to 75-percent tail size. Tail size reductions to 50 percent, 25 percent, and 0 percent also yielded drag decreases but in much smaller increments.

Significant reductions in drag also occurred at Mach 1.20, as shown in figure 13(c). However, the relationship between tail size reduction and drag reduction was considerably more linear. Each tail size reduction generated an approximately equal drag decrease over the entire angle-of-attack range. As expected, the total drag level for each configuration was significantly higher at Mach 1.20 than at lower speeds, primarily because of a large wave-drag contribution.

Nozzle drag accounted for a significant portion of the total aircraft drag. Figure 14 shows the nozzle drag at each Mach number and scheduled NPR as computed from the integration of external static-pressure measurements along the nozzle surfaces. At Mach 0.40 and 0.90, each reduction in tail size produced corresponding reductions in nozzle drag. Tail-size reduction and removal apparently had a favorable effect on afterbody flow-field interactions and produced nozzle drag-reduction increments that were insensitive to angle of attack. However, at Mach 1.20, tail size had only small effects on nozzle drag.

At Mach 0.40 and 1.20, combined horizontal- and vertical-tail size reduction produced a decrease in the lift-curve slope, primarily for the 25-percent and 0-percent tails (fig. 13). As angle of attack increased, the smaller tails generated less lift. However, at Mach 0.90, tail size reductions to 25 percent and 0 percent (tails off) generated a small lift increase over the entire angle-of-attack range. As figure 15 shows, lift on the nozzle was not affected by tail-size reductions. Thus, lift was generated on the remainder of the aircraft and may be a result of the alleviation of adverse wing-afterbody-tail interactions that dominate the transonic flow field for tails that were over 25 percent. There is further discussion of this effect in the sections "Reduction in Horizontal-Tail Size" and "Reduction in Vertical-Tail Size."

The effects of tail size reduction on longitudinal stability are also shown in figure 13. In general, reductions in tail size produced reduced static longitudinal stability. (Static longitudinal stability is defined as the slope of the plot of C_m versus C_L. A configuration is stable if this slope is negative and is more stable for larger negative values.) Although reductions in tail size produced only small effects on lift at Mach 0.40, pitch characteristics were adversely affected. As previously stated, the $\bar{c}/4$ location of each tail size was positioned at a fixed fuselage station to ensure a constant moment reference length for all tail sizes. Thus, the overall changes in aircraft longitudinal stability are directly caused by tail size reductions and by the associated interference effects on the afterbody-tail-jet combination. Similar trends occurred at Mach 0.90, except that there was a much larger downward shift in the zero-lift pitching-moment coefficient (C_{m_0}) with tail size reductions. Relative to the baseline, tail size reductions to

75 percent and 50 percent produced an increase in $C_{m,0}$, while the 25-percent and 0-percent cases decreased zero-lift pitching-moment coefficient. These effects may be caused by wing downwash and afterbody-tail-nozzle interactions that are sensitive to the aft-end geometry. As stated previously, these tail combinations generated increased lift on the afterbody that may have produced the downward shift in $C_{m,0}$.

Although the variation in $C_{m,0}$ was small at Mach 1.20, longitudinal stability also decreased with tail size reduction. However, even with the tails removed, the aircraft remained statically stable throughout the angle-of-attack range. Thus, over the speed range, tail size reductions decreased longitudinal stability, while increases in Mach number resulted in improved stability.

Reduction in vertical-tail size. In addition to reducing the horizontal- and vertical-tail combination, the reduction of vertical-tail size at constant horizontal-tail size was examined. With the horizontal-tail size fixed at 100 percent (full size), data were obtained to isolate the effects of vertical-tail sizes from 100 percent to 0 percent (tails off). Figure 16 shows the longitudinal characteristics over the speed range tested. In general, the reduction in vertical-tail size significantly decreased total drag coefficient at each Mach number. As shown in figure 16(a), the drag increment from vertical-tail size reductions of 100 percent to 50 percent was approximately equal to that measured for further reductions from 50 percent to 0 percent. As figure 17 indicates, vertical-tail size reductions also produced similar effects on nozzle drag coefficient. At Mach 0.40 and 0.90, nozzle drag decreased with vertical-tail size reduction. However, at Mach 1.20, vertical-tail size had little effect on nozzle drag.

Decreases in vertical-tail size also generated small lift increases (fig. 16), particularly at Mach 0.90. This effect was consistent with results discussed previously for combined horizontal- and vertical-tail size combinations. As shown in figure 18, nozzle lift coefficient was independent of vertical-tail size. Thus, the increase in total lift was generated on the remainder of the aircraft, probably as a result of favorable interactions between the wing-afterbody and the horizontal-tail flow field. The induced drag produced by this small lift increase was negligible.

At Mach 0.40 and 0.90, vertical-tail size reduction appeared to have little effect on longitudinal stability characteristics (fig. 16). At Mach 1.20, longitudinal stability increased slightly with tail-size reductions to 50 percent and remained at that value as tails were removed. At transonic and supersonic speeds, a negative $C_{m,0}$ shift occurred which may be a result of additional lift generated on the afterbody from the reduction of vertical-tail size. This shift resulted in lower values of pitching-moment coefficient. Although the lateral-directional stability characteristics were not determined in this study, it is expected that vertical-tail size reduction would degrade lateral-directional stability (ref. 22).

Reduction in horizontal-tail size. The effects of reducing horizontal-tail size on the longitudinal aerodynamic characteristics are shown in figure 19. Vertical-tail size was held constant at 100 percent. In general, horizontal-tail size reductions generated substantial drag coefficient decreases, but these decreases were less than those produced by vertical-tail size reductions. At Mach 0.40, almost all the drag decrease from horizontal-tail removal was generated by the reduction from 100-percent to 50-percent horizontal tails. At transonic and supersonic speeds, each reduction in horizontal-tail size produced approximately equal drag decreases.

The effect of horizontal-tail size on nozzle drag is presented in figure 20 for all three Mach numbers. Data trends were similar to the results for the reduction of vertical-tail size and combined horizontal- and vertical-tail size. At subsonic and transonic speeds, nozzle drag decreased with reduced horizontal-tail size, while at supersonic conditions, nozzle drag increased slightly. However, vertical-tail size reductions (fig. 17) generally produced greater nozzle drag decreases than horizontal-tail size reductions (fig. 20). At Mach 0.40 and 0.90, changes in vertical-tail size obviously produced more favorable afterbody flow-field effects.

Over the speed range, lift coefficient was independent of horizontal-tail size at angles of attack less than 2° (fig. 19). At angles of attack over 2°, lift decreased as horizontal-tail size (and available lifting-surface area) was reduced. In contrast, vertical-tail size reductions produced lift increases. As discussed previously for the combined horizontal- and vertical-tail case, the combination of these effects produced a decrease in the lift-curve slope, primarily for the 25- and 0-percent tails at Mach 0.40 and 1.20. The favorable effects on the wing-afterbody-tail flow field of vertical-tail size reduction were cancelled by the unfavorable effects on lift of horizontal-tail size reduction. However, at Mach 0.90, the favorable lift effects of vertical-tail size reduction dominated as both tails were reduced to 25 percent and 0 percent. Reductions in vertical-tail size alleviated the adverse interference effects from the horizontal tails to produce an aft-end lift increase and a resulting decrease in

pitching-moment coefficient. As shown in figure 21, nozzle lift was independent of horizontal-tail size.

As expected, longitudinal stability characteristics (fig. 19) were significantly affected by reductions in horizontal-tail size. Over the speed range, decreases in horizontal-tail size reduced longitudinal stability. As a result of reductions in lifting-surface area, $C_{m,0}$ also increased as horizontal-tail size decreased. At Mach 1.20, similar trends occurred, but even without the horizontal tails the configuration remained statically stable. Throughout the speed range, the effects of horizontal-tail size reductions followed trends similar to the longitudinal stability characteristics of combined horizontal- and vertical-tail size reductions discussed previously. Vertical-tail size reductions produced no significant effects on longitudinal stability. Thus, the reduction in lifting-surface area from horizontal-tail size reductions produced a much greater effect on longitudinal stability than vertical-tail size reductions.

Detailed Drag Data Comparisons at $\alpha = 0°$

Combined horizontal- and vertical-tail size reductions. The effects of reduced horizontal- and vertical-tail sizes on total drag and nozzle drag at 0° angle of attack are shown in figures 22 and 23. In general, total drag decreased significantly with tail size reduction. As Mach number increased, total drag also increased, particularly at supersonic speeds. However, the reduction in total drag coefficient with tail size also increased with Mach number. The reduction in total drag coefficient from full tails to tails off was approximately 0.0040 at Mach 0.40, 0.0050 at Mach 0.90, and 0.0080 at Mach 1.20. As a result of the reduced surface area of each tail size, the tail skin-friction drag contribution to total drag also decreased.

Nozzle drag (fig. 23) also increased with Mach number, but at transonic speeds ($M = 0.90$), tail size reductions produced significant nozzle drag reductions to levels below those at Mach 0.40. At Mach 0.90, tail reductions to 50 percent produced favorable afterbody-tail-nozzle interactions that substantially reduced nozzle drag. Further tail size reductions to 0 percent (tails off) did not produce significant changes. At supersonic speeds, tail size reduction had no significant effect on nozzle drag.

A summary of the percent total drag reduction (relative to the baseline configuration) produced by tail size reductions is shown in figure 24 with a breakdown of the component contributions. In general, total drag reduction increased with each tail size decrease. The removal of all tails produced approximately 15-percent total drag reduction over the entire speed range. At subsonic and transonic speeds, approximately half the drag reduction produced by removing all tails was achieved by tail size reductions to 75 percent. Tail size reductions to 50 percent also produced a significant drag decrease relative to the baseline. Tail size reductions to 25 percent and 0 percent also produced further drag decreases but in smaller increments. However, at Mach 1.20, each tail size reduction produced an approximately equal decrease in total drag. Although tail interference effects were negligible, the wave drag of the tails was significantly reduced.

Several factors contributed to the significant drag decreases produced by tail size reductions. Tail size changes affected the tail skin-friction drag and tail interference-drag contributions at subsonic speeds and tail wave drag at supersonic speeds. Of these factors, only the tail interference terms represent more than just the direct effects of surface area and volume reduction that are the basis of the skin-friction and wave-drag terms. Figure 24 also shows the effects of reducing horizontal- and vertical-tail size on the tail interference-drag increments. The tail interference-drag increments on the nozzles and on the remainder of the fuselage are presented. At subsonic and transonic speeds, reducing tail size produced a substantial tail interference-drag reduction that was the largest for the 50-percent tails. Tail size reduction from 100 percent to 25 percent and 0 percent actually produced less favorable effects on tail interference drag than size reductions to 75 percent and 50 percent. At these speeds, a large portion of the tail interference-drag reduction was the result of favorable interference effects on the nozzles. As tail size decreased, the total drag reduction due to tail interference effects on the nozzles continued to increase while it decreased for the remainder of the aircraft. As expected, the tail interference-drag effects were largest at transonic speeds, where a complex afterbody flow field exists. At Mach 1.20, the effect of tail size on tail interference drag was relatively small.

Reduction of vertical-tail size. The effects of reductions in vertical-tail size on the total drag coefficient are presented in figure 25. The data indicate a significant reduction in total drag at all test speeds as vertical-tail size was reduced. Since the incremental drag reduction was approximately equal for each size decrease, the payoffs of completely removing the vertical tails are substantial. Figure 26 shows similar effects on nozzle drag coefficient at subsonic speeds. However, at Mach 0.90 and 1.20, the nozzle flow field was sensitive to specific tail arrangements. Vertical-tail size reductions adversely

influenced nozzle flow-field interactions to produce slight increases in nozzle drag at supersonic speeds.

A summary of the percent reduction in total drag coefficient (relative to the baseline configuration) that results from reductions in vertical-tail size is shown in figure 27. The removal of vertical tails entirely produced a 10- to 13-percent total drag reduction over the entire speed range. The largest drag reduction occurred at Mach 0.90. At this condition, most of the drag reduction was a result of favorable tail interference effects on the afterbody flow field, particularly on the nozzles. Tail interference effects were small with the vertical tail removed at supersonic speeds, but tail wave drag significantly decreased to produce a substantial total drag reduction.

Reduction of horizontal-tail size. The effects of reduced horizontal-tail size on total drag coefficient are shown in figure 28. In general, reductions in horizontal-tail size produced substantial decreases in total drag coefficient over the speed range tested. Nozzle drag coefficient, as shown in figure 29, followed similar trends at Mach 0.40 and 0.90, in that nozzle drag decreased as horizontal-tail size decreased. At Mach 1.20, the effects of horizontal-tail size on nozzle drag were small.

The effects of horizontal-tail size on total drag coefficient reduction and the relative contributions are shown in figure 30. At subsonic and transonic speeds, horizontal-tail size reductions generated favorable interactions on the entire aircraft. At supersonic speeds, tail size reductions produced no significant tail interference effects. Vertical-tail size reductions (fig. 27) produced larger decreases in total drag than horizontal-tail size reductions (fig. 30). Over the speed range, removing the horizontal tails produced a total drag reduction from 6 to 9 percent. Although the horizontal tails had slightly smaller surface areas than the vertical tails, this drag reduction was considerably less than the 10- to 13-percent drag decrease generated by complete removal of the vertical tails. The drag-reduction efficiency of the vertical tails was much greater than that of the horizontal tails. Vertical-tail removal also produced a small lift increase on the afterbody as opposed to a decrease with horizontal-tail removal.

Summary of Drag Effects for All Tail Combinations

A summary of the total drag reduction produced by all the tail combinations and their relative drag reduction efficiencies are presented in table 3. Figure 31 graphically depicts the total drag reduction percentages from table 3, while figure 32 presents the drag reduction efficiency of each tail combination. In figure 32, the horizontal axis represents the percent tail area reduction relative to the baseline 100-percent tails. Therefore, a 75-percent tail area reduction is equal to a 25-percent tail size. The dotted line represents a linear relationship between tail area reduction and drag reduction. For example, a 50-percent reduction in tail area would produce a 50-percent reduction in drag. In general, removing all tails produced the largest reduction in total drag at all test speeds. Removing the vertical tails was much more effective at reducing drag than was the removal of horizontal tails. At Mach 0.40, total drag coefficient decreased significantly by reducing both tails to 50 percent. Approximately 80 percent of the drag reduction from removing all tails was achieved by reducing both tails to 50 percent (fig. 32(a)). This drag reduction was also greater than for the removal of horizontal and vertical tails separately. However, at Mach 0.90 (fig. 32(b)), removing the vertical tails generated favorable tail interference effects that produced a 13.25-percent total drag reduction, or 86 percent of that generated with all tails removed. The removal of the vertical tails even produced a drag reduction slightly larger than that generated by reducing both tails to 25 percent. Other than the removal of all tails, the elimination of the vertical tails produced the largest drag reduction and highest efficiency at transonic speeds.

At Mach 1.20, the removal of vertical tails also produced significant drag decreases that were slightly greater than with the 25-percent tails. As table 3 and figure 32 indicate over the speed range, removing the vertical tails generated from 68 percent to 86 percent of the total drag reduction from removing all tails. Removing the vertical tails also generated considerably more drag reduction than the removal of horizontal tails. However, the combined tail size reduction to 25 percent was much more effective at low speeds. Over the speed range, the 25-percent tails produced from 70 to 85 percent of the total drag from removing all tails. Therefore, the reduction in horizontal- and vertical-tail sizes to 25 percent was the most effective tail arrangement at reducing drag other than the removal of all tails.

Conclusions

An investigation was conducted in the Langley 16-Foot Transonic Tunnel to determine the effects of reduced horizontal- and vertical-tail sizes on the longitudinal aerodynamic characteristics of a modified F-15 model with canards and two-dimensional convergent-divergent thrust-vectoring nozzles. This study focused primarily on quantifying the drag

decrease at low angles of attack from tail size reductions. Data were obtained on the baseline configuration with and without tails and with reduced horizontal- and/or vertical-tail sizes that were 75, 50, and 25 percent of the baseline tail areas. The model was tested at Mach numbers of 0.40, 0.90, and 1.20 over an angle of attack range from $-2°$ to $10°$. Nozzle pressure ratio was varied from 1.0 (jet off) to 7.5. Results from this study indicated the following:

1. The reduction or elimination of horizontal and vertical tails produced a reduction in total aircraft drag of up to approximately 16 percent. Tail size reduction produced favorable effects on the afterbody-tail-nozzle flow field that reduced skin-friction drag, tail interference drag, and wave drag.

2. Generally, the relationship between tail size reduction and total drag reduction was not linear.

3. Other than the removal of all tails, the 25-percent horizontal- and vertical-tail combination was the most effective at producing the largest drag decrease over the entire speed range. Tail size reductions to 25 percent produced from 70 to 85 percent of the drag decrease produced with tails off. Reductions in tail sizes to 50 percent generated from 49 to 78 percent of the total drag reduction possible.

4. At transonic speeds, tail interference drag decreased significantly for all tail combinations, particularly as the vertical tails were removed. Tail size reduction improved the afterbody-nozzle-tail flow field to reduce nozzle drag.

5. Removing the vertical tails was much more effective at reducing total drag than removing the horizontal tails. With the exception of all tails removed, the elimination of the vertical tails was the most effective tail arrangement at transonic and supersonic speeds.

6. Over the entire speed range, decreases in combined horizontal- and vertical-tail size generated reduced longitudinal stability, primarily as a result of horizontal-tail size effects. Vertical-tail size reduction produced no significant effects on longitudinal stability; however, removing the vertical tails produced a small lift increase on the afterbody and a resulting decrease in pitching-moment coefficient.

NASA Langley Research Center
Hampton, VA 23665-5225
June 18, 1990

References

1. Herbst, W. B.: Future Fighter Technologies. *J. Aircr.*, vol. 17, no. 8, Aug. 1980, pp. 561–566.
2. Well, K. H.; Faber, B.; and Berger, E.: Optimization of Tactical Aircraft Maneuvers Utilizing High Angles of Attack. *J. Guid., Control, & Dyn.*, vol. 5, no. 2, Mar.–Apr. 1982, pp. 131–137.
3. Skow, Andrew M.; Hamilton, William L.; and Taylor, John H.: Advanced Fighter Agility Metrics. AIAA-85-1779, Aug. 1985.
4. Herrick, Paul W.: Air Combat Payoffs of Vectoring/ Reversing Exhaust Nozzles. AIAA-88-3239, July 1988.
5. Nelson, B. D.; and Nicolai, L. M.: Application of Multi-Function Nozzles to Advanced Fighters. AIAA-81-2618, Dec. 1981.
6. Pennington, J. E.; and Meintel, A. J., Jr.: Performance and Human Factors Results From Thrust Vectoring Investigations in Simulated Air Combat. Proceedings of the 1980 Joint Automatic Control Conference, Volume 1, IEEE: 80CH1580-0, American Automatic Control Council, c.1980, Paper TA1-A.
7. Lacey, David W.: Air Combat Advantages From Reaction Control Systems. SAE Tech. Paper Ser. 801177, Oct. 1980.
8. Henderson, William P.: Propulsion Integration for Military Aircraft. SAE Tech. Paper 892234, Sept. 1989.
9. Capone, Francis J.; and Mason, Mary L.: *Multiaxis Aircraft Control Power From Thrust Vectoring at High Angles of Attack.* NASA TM-87741, 1986.
10. Berrier, Bobby L.: Results From NASA Langley Experimental Studies of Multiaxis Thrust Vectoring Nozzles. SAE 1988 Transactions—Journal of Aerospace, Section 1—Volume 97, c.1989, pp. 1.1289–1.1304. (Available as SAE Paper 881481.)
11. Leavitt, Laurence D.: *Effect of Empennage Location on Twin-Engine Afterbody/Nozzle Aerodynamic Characteristics at Mach Numbers From 0.6 to 1.2.* NASA TP-2116, 1983.
12. Leavitt, Laurence D.; and Bare, E. Ann: *Effects of Twin-Vertical-Tail Parameters on Twin-Engine Afterbody/Nozzle Aerodynamic Characteristics.* NASA TP-2158, 1983.
13. Leavitt, Laurence D.: Effects of Various Empennage Parameters on the Aerodynamic Characteristics of a Twin-Engine Afterbody Model. AIAA-83-0085, Jan. 1983.
14. Berrier, Bobby L.: Empennage/Afterbody Integration for Single and Twin-Engine Fighter Aircraft. AIAA-83-1126, June 1983.
15. Mello, J. F.; and Kotansky, D. R.: Aero/Propulsion Technology for STOL and Maneuver. AIAA-85-4013, Oct. 1985.
16. Peddrew, Kathryn H., compiler: *A User's Guide to the Langley 16-Foot Transonic Tunnel.* NASA TM-83186, 1981.
17. Braslow, Albert L.; Hicks, Raymond M.; and Harris, Roy V., Jr.: *Use of Grit-Type Boundary-Layer-Transition Trips on Wind-Tunnel Models.* NASA TN D-3579, 1966.
18. Braslow, Albert L.; and Knox, Eugene C.: *Simplified Method for Determination of Critical Height of Distributed Roughness Particles for Boundary-Layer Transition at Mach Numbers From 0 to 5.* NACA TN 4363, 1958.
19. Shapiro, Ascher H.: *The Dynamics and Thermodynamics of Compressible Fluid Flow, Volume II.* Ronald Press Co., c.1954.
20. Mercer, Charles E.; Berrier, Bobby L.; Capone, Francis J.; Grayston, Alan M.; and Sherman, C. D.: *Computations for the 16-Foot Transonic Tunnel—NASA, Langley Research Center, Revision 1.* NASA TM-86319, 1987. (Supersedes NASA TM-86319, 1984.)
21. Harris, Roy V., Jr.: *An Analysis and Correlation of Aircraft Wave Drag.* NASA TM X-947, 1964.
22. Murri, Daniel G.; Grafton, Sue B.; and Hoffler, Keith D.: *Wind-Tunel Investigation and Free-Flight Evaluation of a Model of the F-15 STOL and Maneuver Technology Demonstrator*, NASA TP-3003, 1990.

Table 1. Model Geometry

Wing geometry:	
Airfoil sections	NACA 64AXXX with modified cambered leading edge
At root section	NACA 64A(5.5)(05.9)
At 43.4-percent span	NACA 64A(5.5)(04.6)
At 82.1-percent span	NACA 64A2(03.5)
At tip section	NACA 64A203
Reference area, in^2	608.00
Span, in.	42.80
Mean aerodynamic chord, in.	15.942
Tip chord, in.	5.695
Root chord, in.	22.766
Taper ratio	0.250
Aspect ratio	3.013
LE sweep angle, deg	45.0
Dihedral angle, deg	−1.0
Canard geometry:	
Airfoil sections	Modified NACA 64-000X
At root section	NACA 64-0006
At tip section	NACA 64-0002
Area (each), in^2	87.93
Span (each), in.	7.33
Root chord, in.	8.532
Tip chord, in.	3.787
Aspect ratio	2.44
Taper ratio	0.46
LE sweep angle, deg	47.16
Dihedral angle, deg	+20.0
Horizontal-tail geometry:	
Airfoil sections	Modified NACA 64A-000X
At root section	NACA 64A-0005.5
At 21.3-percent span	NACA 64A-0003.5
At tip section	NACA 64A-0002.5
Area (each), in^2	59.904
Span, in.	7.830
Root chord, in.	11.429
Tip chord, in.	3.873
Taper ratio	0.339
Aspect ratio	2.046
LE sweep angle, deg	50.0
Dihedral angle, deg	0.0
Vertical-tail geometry:	
Airfoil sections	Modified NACA 64-000X
At root section	NACA 64-0005
At tip section	NACA 64-0003.5
Area (each), in^2	62.496
Span (each), in.	10.313
Root chord, in.	9.580
Tip chord, in.	2.549
Taper ratio	0.266
Aspect ratio	1.70
LE sweep angle	36.57
Toe angle (LE out), deg	2.0

Table 2. Test Matrix

Config.	δ_c, deg	HT size, percent	δ_{ht}, deg	VT size, percent	δ_r, deg	Mach	α, deg	NPR	$\delta_{v,y}$, deg
1 (Baseline)	−5/− 5	100	0/0	100	0/0	0.4	0	1.0 to 4.0	0/0
						.4	−2 to 10	3.8	
						.9	0	1.0 to 6.5	
						.9	−2 to 10	5.6	
						1.2	0	1.0 to 8.8	
							−2 to 10	7.5	
2	−5/− 5	75	0/0	75	0/0	0.4	−2 to 10	3.5	0/0
						.9		5.7	
						1.2		7.5	
3	−5/− 5	50	0/0	50	0/0	0.4		3.7	0/0
						.9		5.7	
						1.2		7.5	
4	−5/− 5	25	0/0	25	0/0	0.4		3.5	0/0
						.9		5.7	
						1.2		7.5	
5	−5/− 5	0	0/0	0	0/0	0.4	0	1.0 to 3.5	0/0
						.4	−2 to 10	3.2	
						.9	0	1.0 to 5.5	
						.9	−2 to 10	4.8	
						1.2	0	1.0 to 8.5	
						1.2	−2 to 10	7.5	
6	−5/− 5	100	0/0	50	0/0	0.4	−2 to 10	3.7	0/0
						.9		5.6	
						1.2		7.5	
7	−5/− 5	100	0/0	0	0/0	0.4	−2 to 10	3.4	0/0
						.9		4.9	
						1.2		7.1	
8	−5/− 5	50	0/0	100	0/0	0.4	−2 to 10	3.7	0/0
						.9		5.6	
						1.2		7.5	
9	−5/− 5	0	0/0	100	0/0	0.4	−2 to 10	3.8	0/0
						.9		5.7	
						1.2		7.5	

Table 3. Summary of Drag Reduction at $\alpha = 0°$

Tail size (%HT/%VT)	Drag reduction at $\alpha = 0°$ relative to baseline, deg			Tail-exposed surface area reduction, ft^2	Drag reduction efficiency (C_D reduction relative to baseline / Maximum C_D reduction (tails off))		
	$M = 0.40$	$M = 0.90$	$M = 1.20$		$M = 0.40$	$M = 0.90$	$M = 1.20$
75/75	6.47	7.89	3.95	0.85 (25%)	0.44	0.51	0.27
50/50	11.51	11.99	7.36	1.70 (50%)	.78	.78	.49
25/25	12.59	12.93	10.41	2.55 (75%)	.85	.84	.70
0/0	14.75	15.46	14.90	3.40 (100%)	1.00	1.00	1.00
100/50	4.68	5.36	4.13	.87 (26%)	.32	.35	.28
100/0	10.07	13.25	10.59	1.74 (51%)	.68	.86	.71
50/100	6.12	5.68	3.05	.83 (24%)	.41	.37	.20
0/100	7.91	8.83	5.57	1.66 (49%)	.54	.57	.37

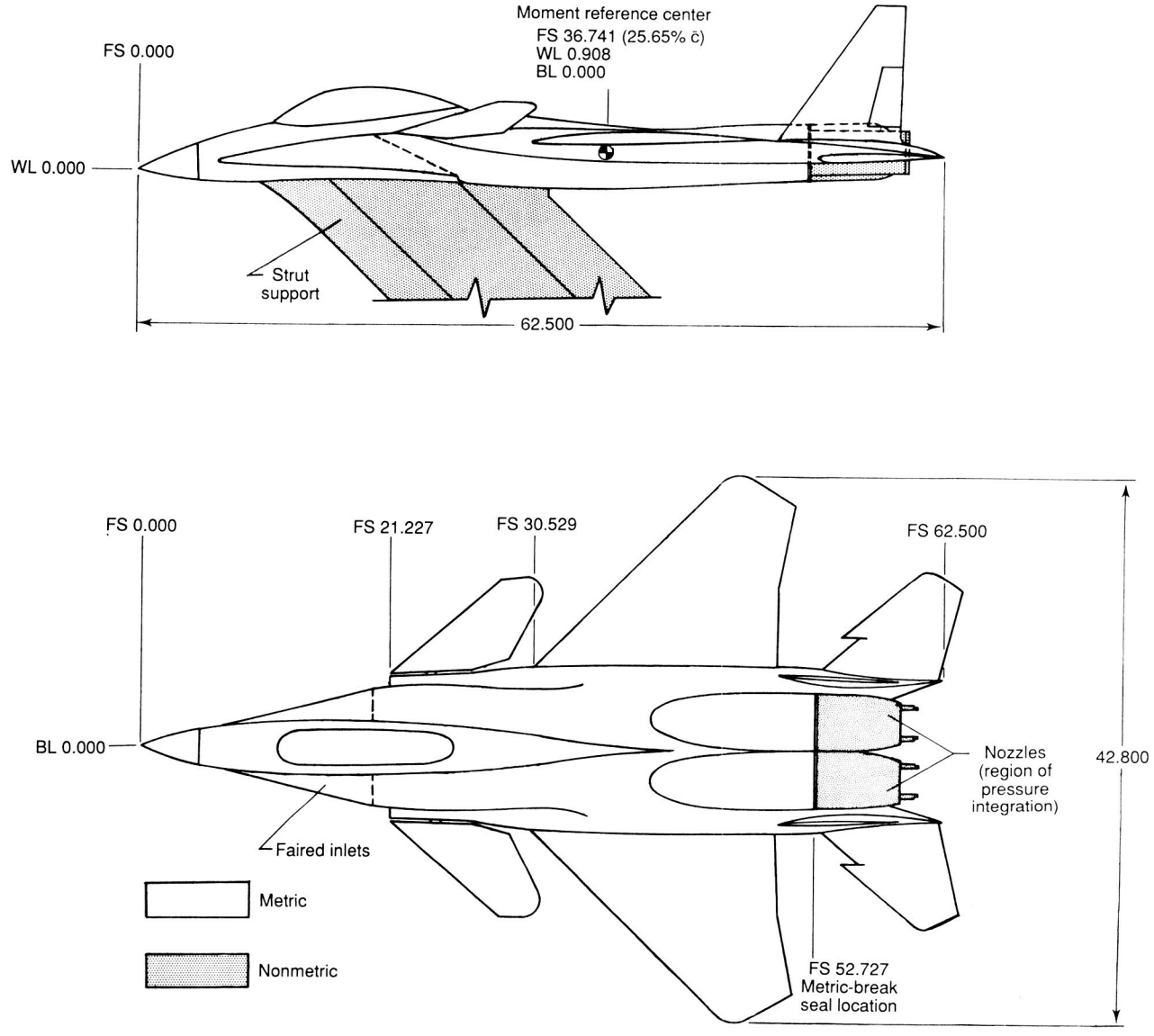

Figure 1. Details of model geometry. (See table 1.) All linear dimensions are in inches.

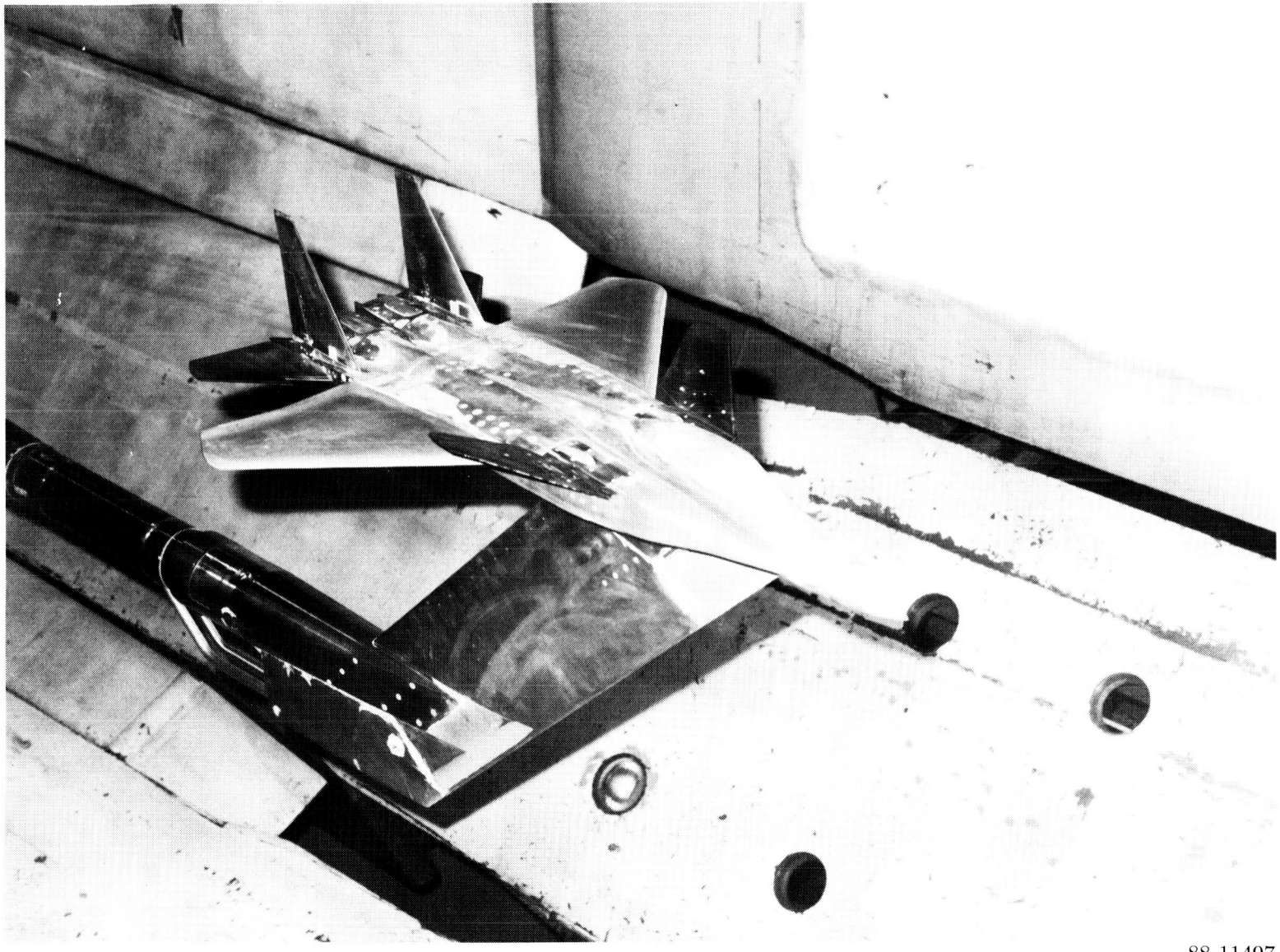

88-11497

Figure 2. Baseline F-15 S/MTD configuration with 100-percent tails installed in Langley 16-Foot Transonic Tunnel.

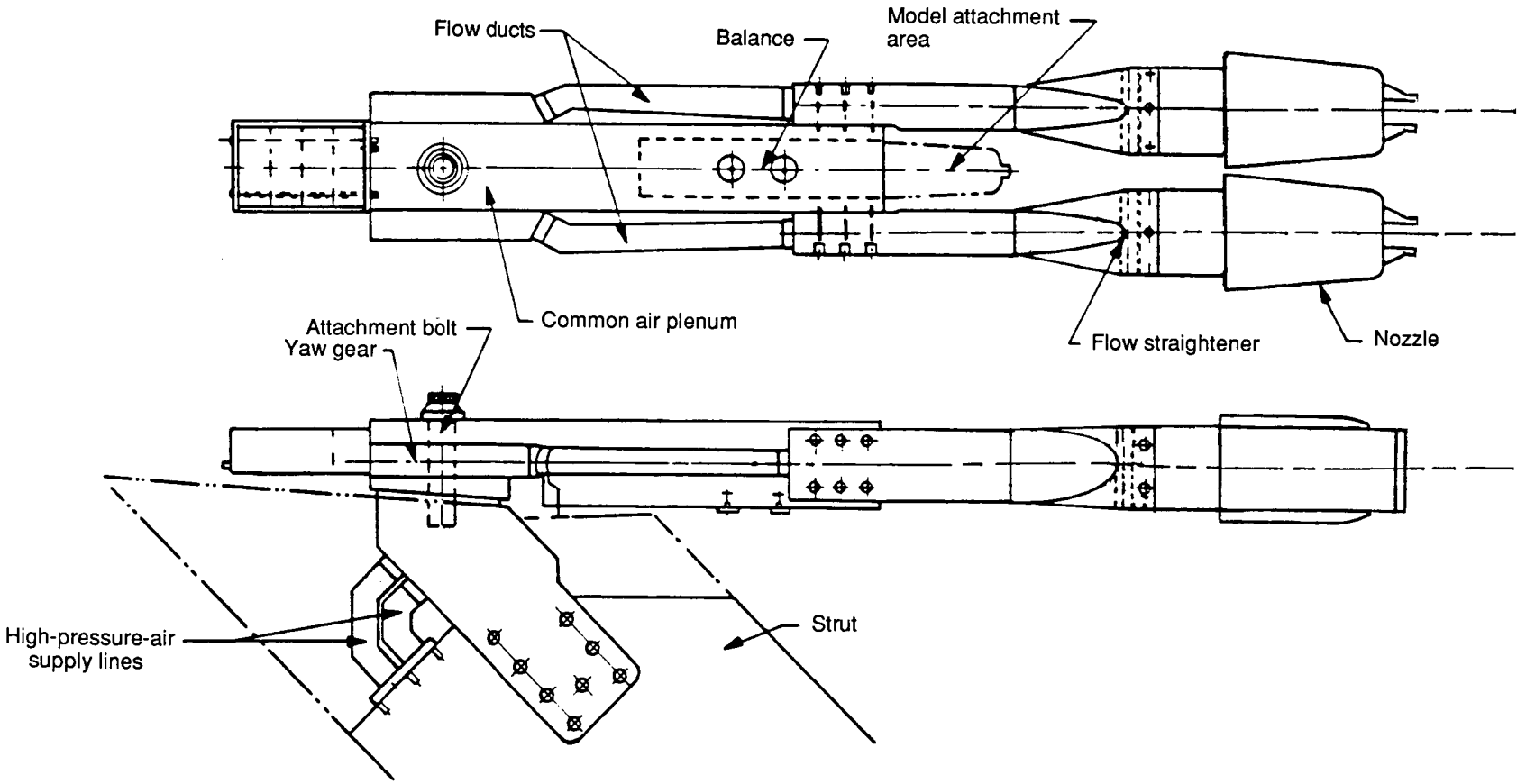

Figure 3. Nonmetric twin-engine propulsion system with 2-D C-D nozzles.

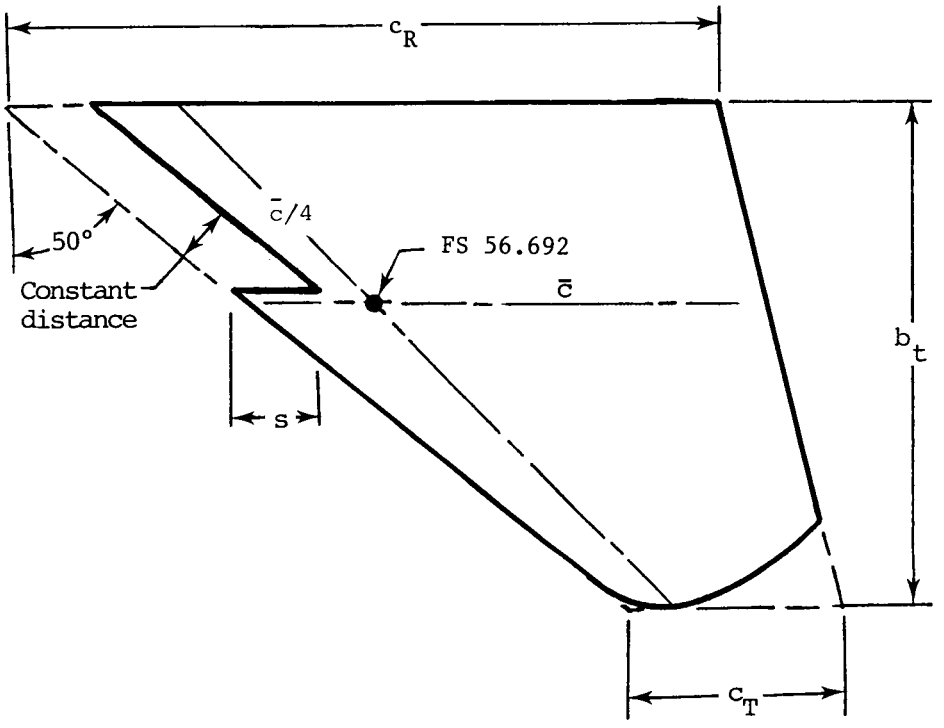

Airfoil sections:

At c_R : NACA 64A-0005.5
At 21.3% b_t: NACA 64A-0003.5
At c_T : NACA 64A-0002.5

Tail size, percent area	Surface area per side, ft^2	Span, b_t, in.	Root chord, c_R, in.	Tip chord, c_T, in.	Mean aero. chord, $\bar{c}$, in.	Slot length, s, in.
100	0.416	7.830	11.429	3.873	8.272	1.424
75	.312	6.781	9.898	3.355	7.164	1.233
50	.208	5.537	8.081	2.739	5.849	1.007
25	.104	3.915	5.714	1.937	4.136	.712

Figure 4. Dimensions of horizontal tail.

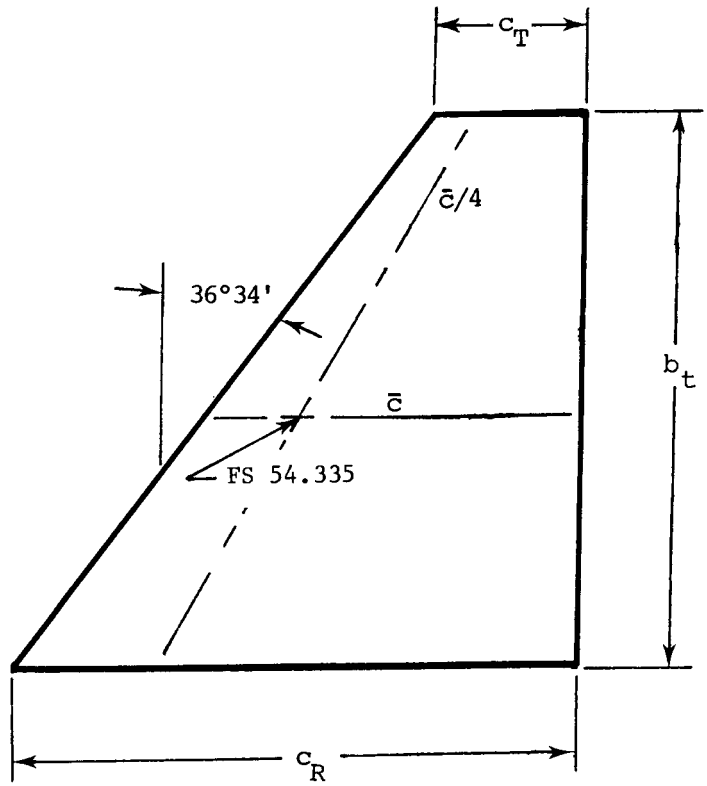

Airfoil sections:

At c_R: NACA 64-0005
At c_T: NACA 64-0003.5

Tail size, percent area	Surface area per side, ft^2	Span, b_t, in.	Root chord, c_R, in.	Tip chord, c_T, in.	Mean aero. chord, $\bar{c}$, in.
100	0.434	10.313	9.580	2.549	6.747
75	.326	8.931	8.296	2.208	5.843
50	.217	7.292	6.774	1.802	4.771
25	.109	5.156	4.790	1.275	3.374

Figure 5. Dimensions of vertical tail.

88-11489

Figure 6. Installed model with 50-percent horizontal and vertical tails.

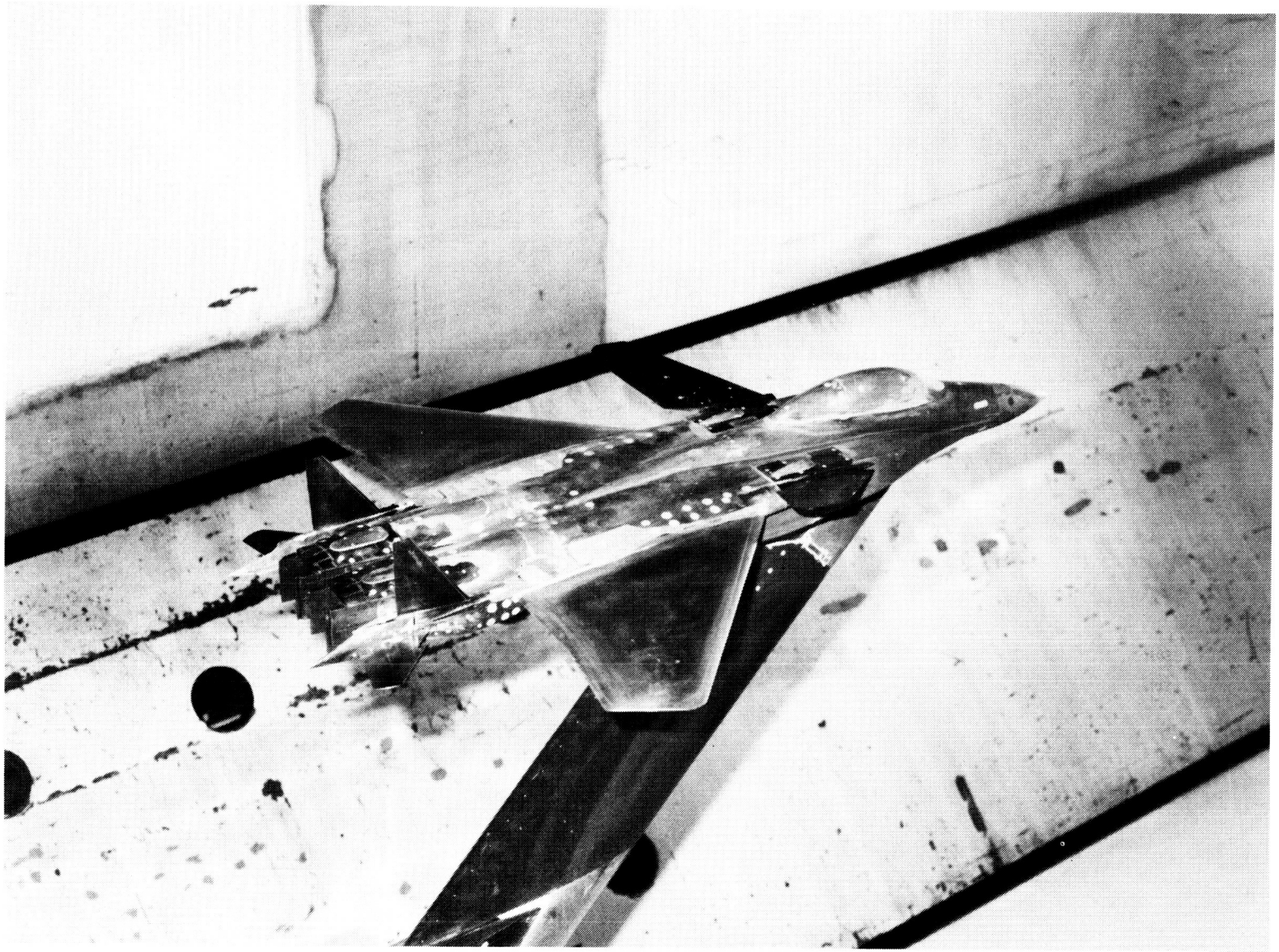

88-11499

Figure 7. Installed model with 25-percent horizontal and vertical tails.

88-11493

Figure 8. Installed model with horizontal and vertical tails removed.

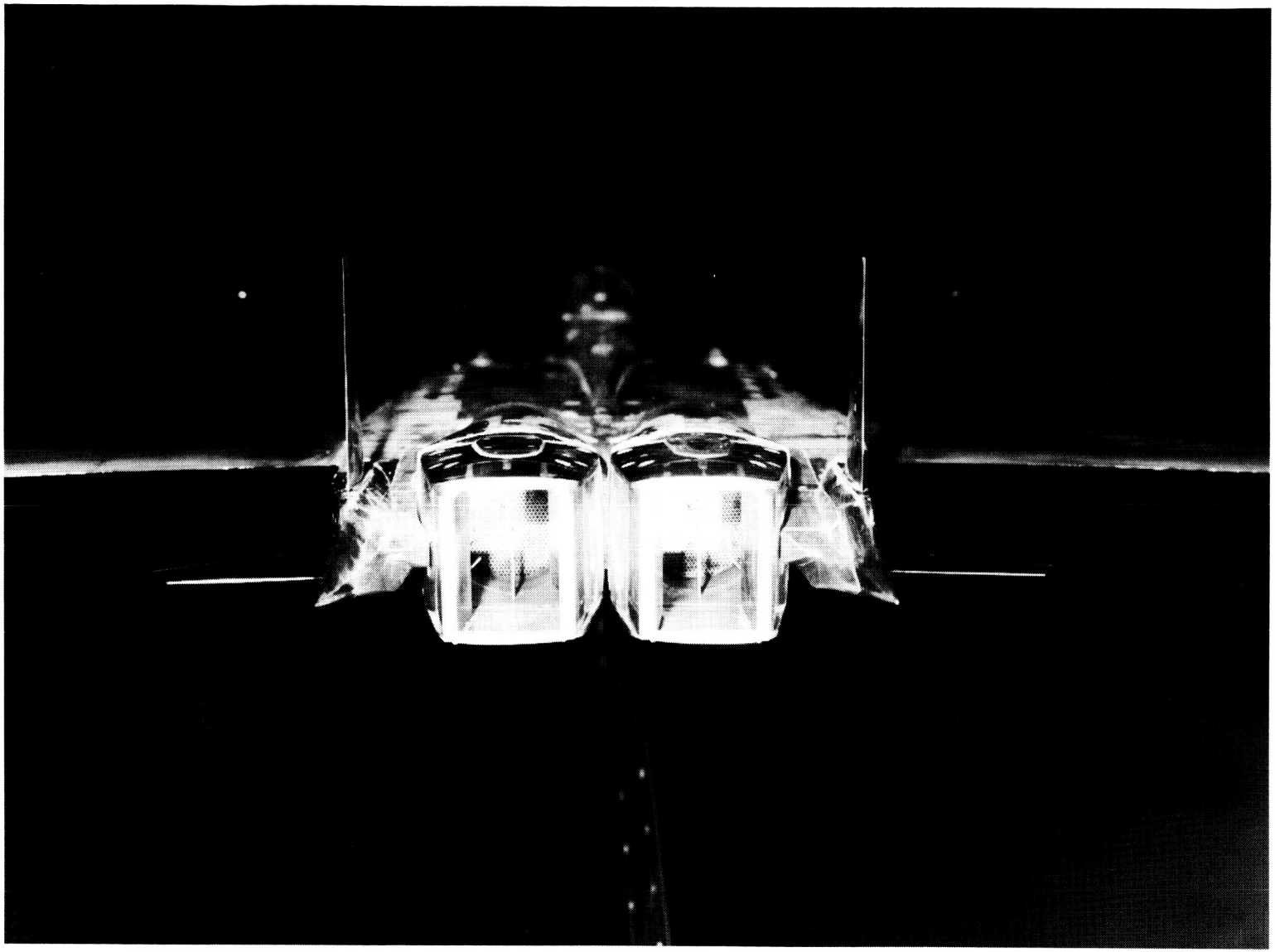

88-11488

Figure 9. Aft-end view of two-dimensional nozzles with 25-percent horizontal and vertical tails.

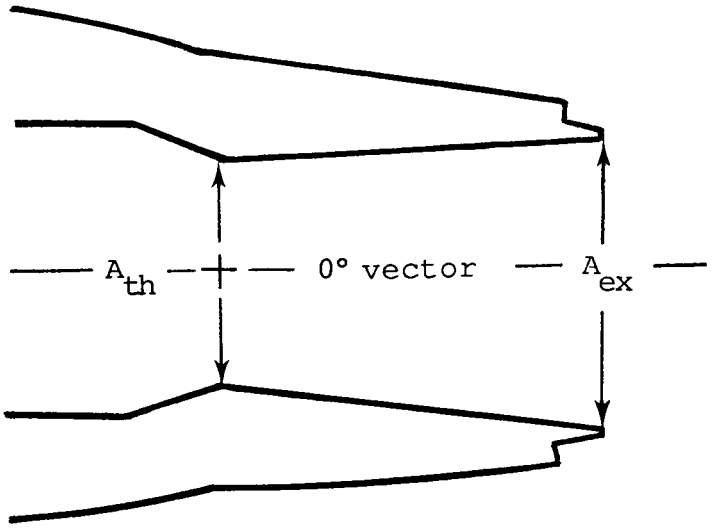

Figure 10. Top view of internal geometry of a low mach, 2-D C-D, A/B nozzle. $A_{th} = 5.20$; $A_{ex} = 6.60$; $\epsilon = 1.269$; Design NPR = 4.397.

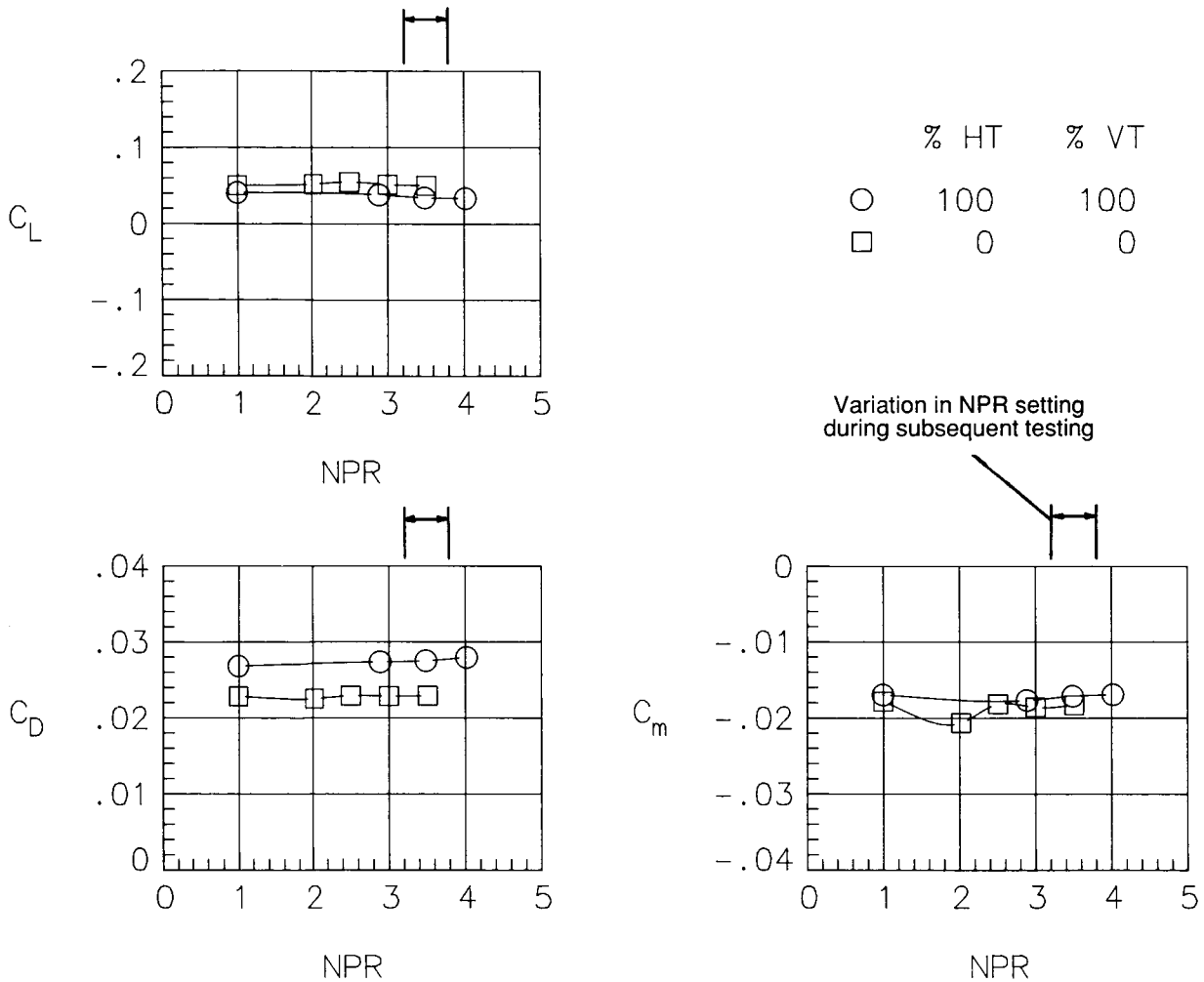

(a) $M = 0.40$.

Figure 11. Effects of nozzle pressure ratio on longitudinal aerodynamic characteristics; $\alpha = 0°$.

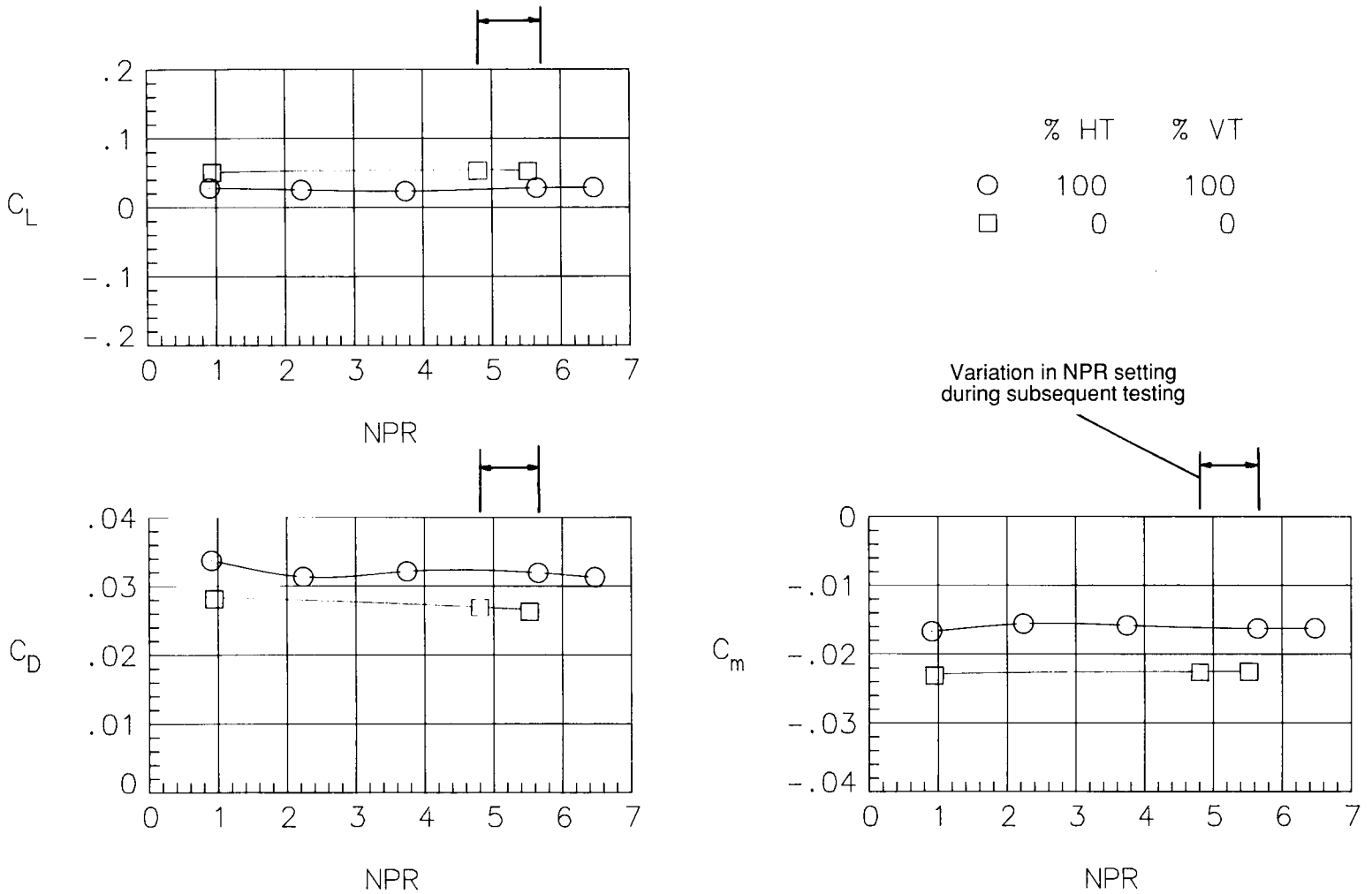

(b) $M = 0.90$.

Figure 11. Continued.

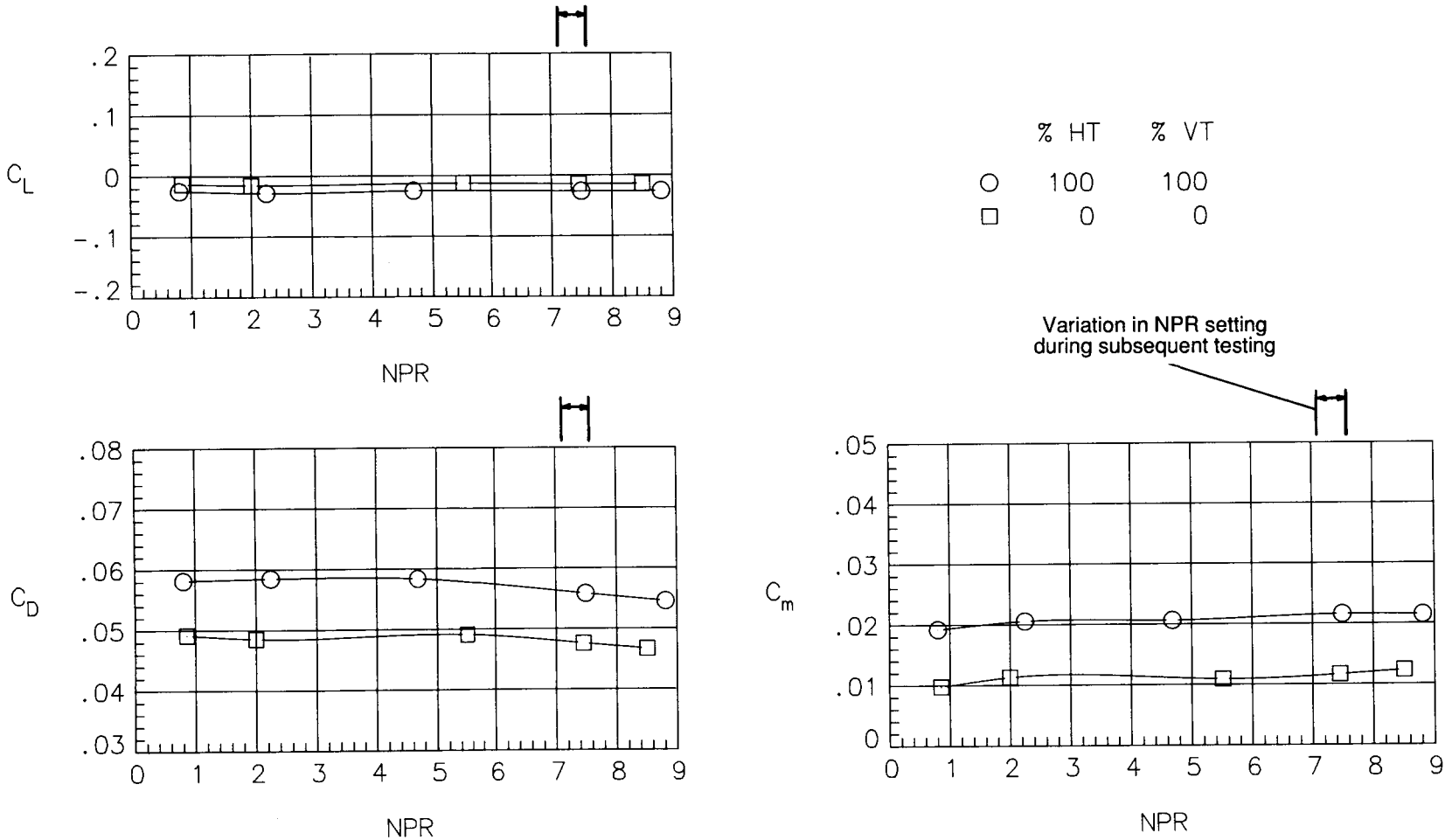

(c) $M = 1.20$.

Figure 11. Concluded.

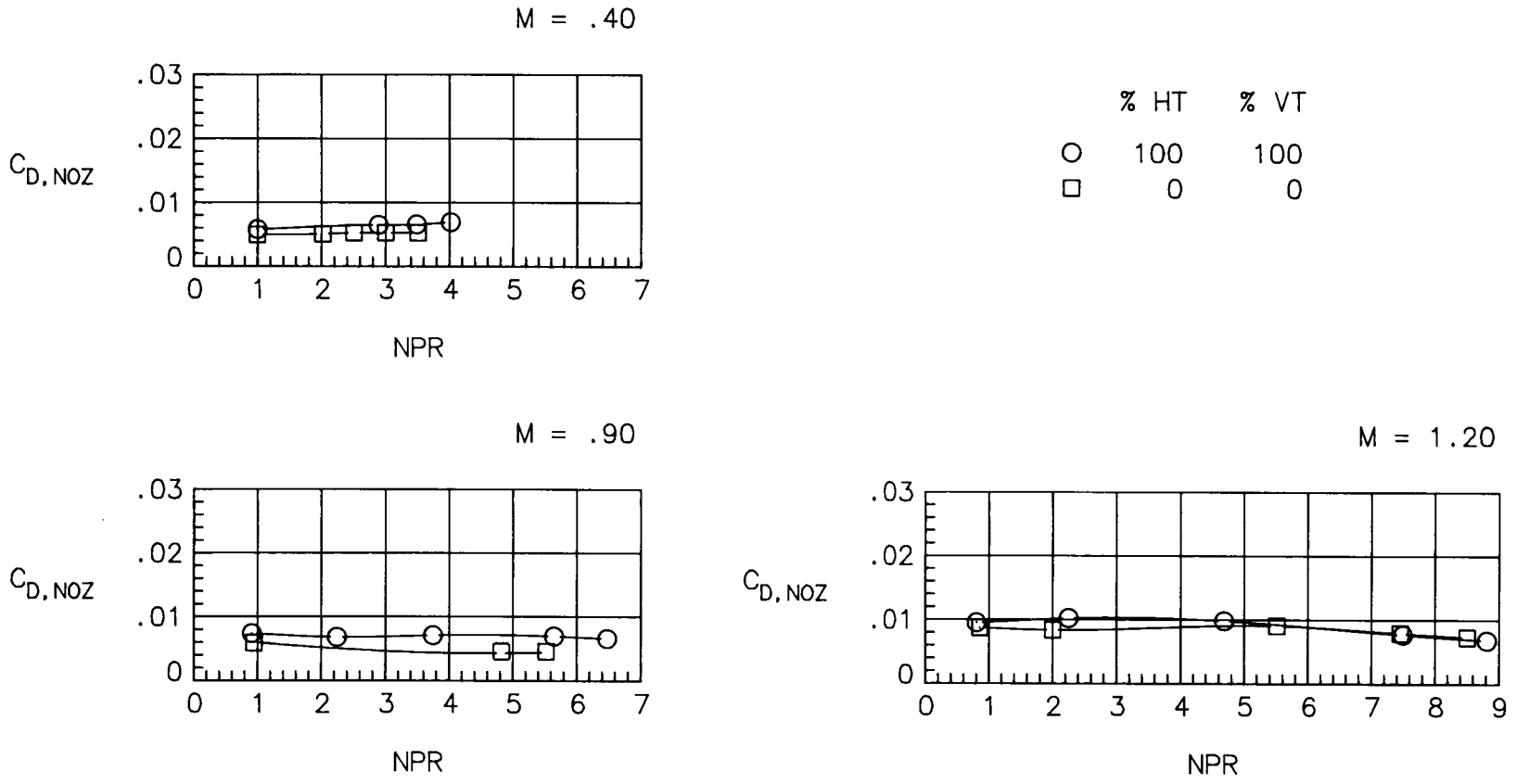

Figure 12. Effects of nozzle pressure ratio on nozzle drag coefficient; $\alpha = 0°$.

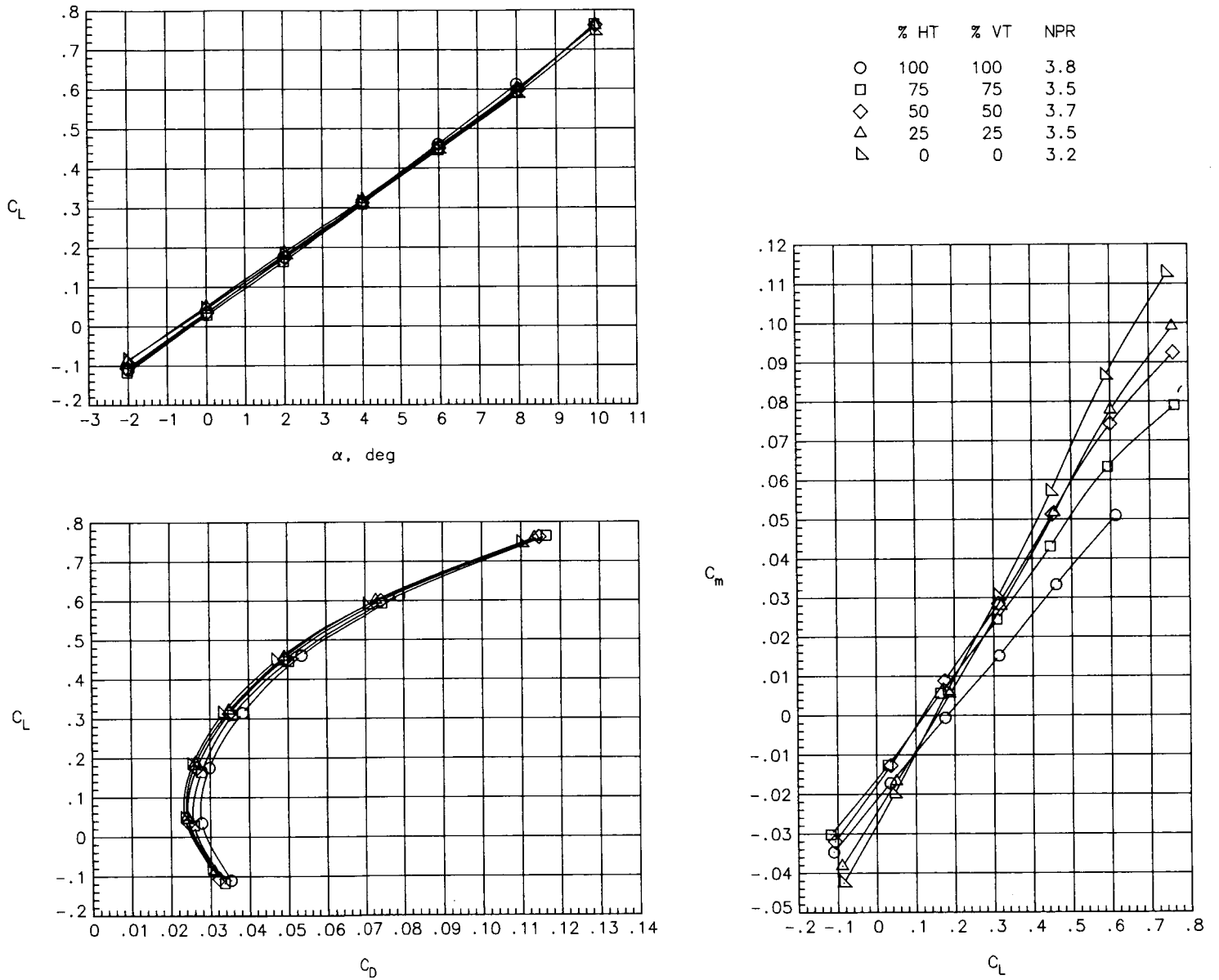

(a) $M = 0.40$.

Figure 13. Effects of horizontal- and vertical-tail size on longitudinal aerodynamic characteristics.

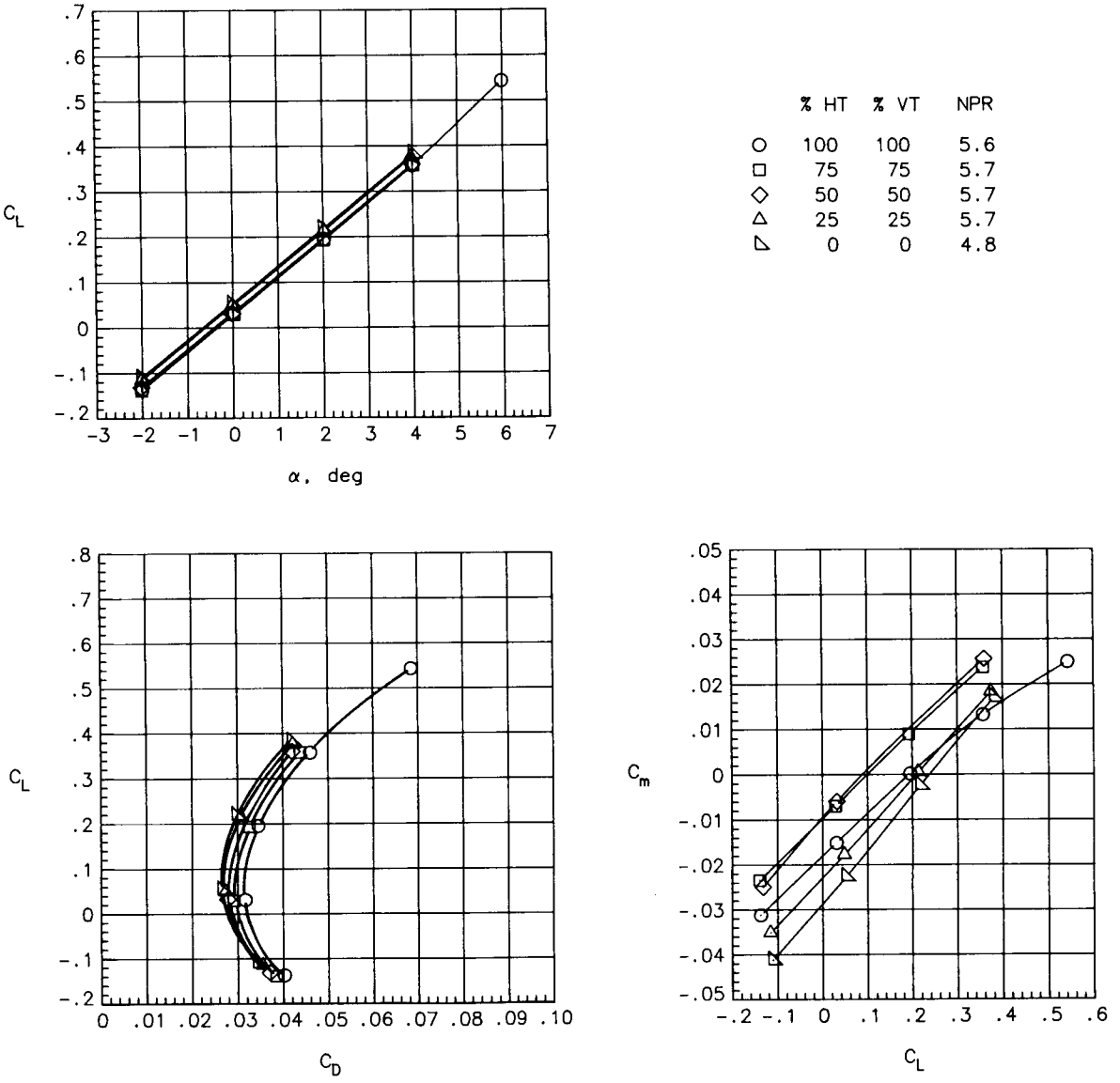

(b) $M = 0.90$.

Figure 13. Continued.

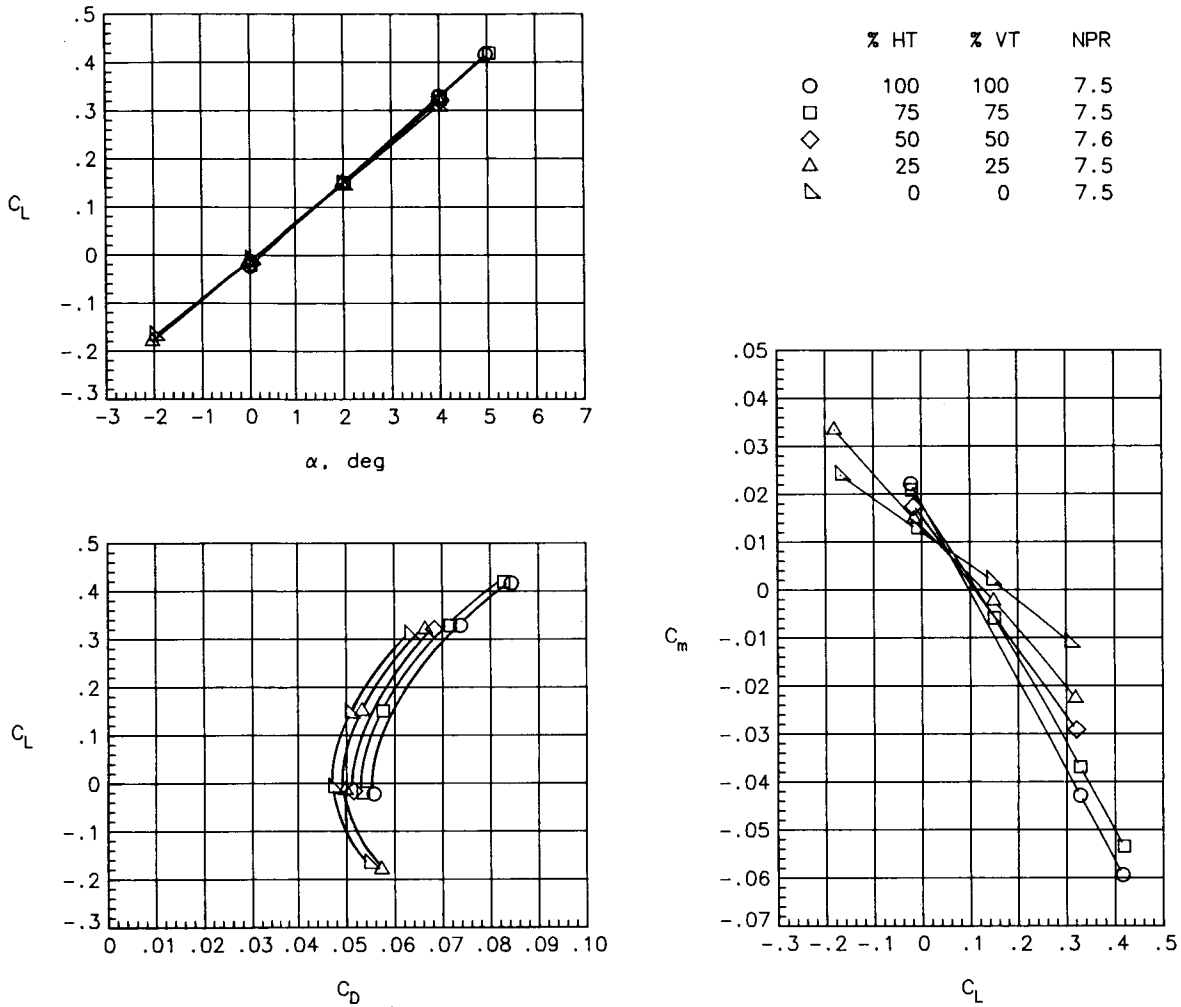

(c) $M = 1.20$.

Figure 13. Concluded.

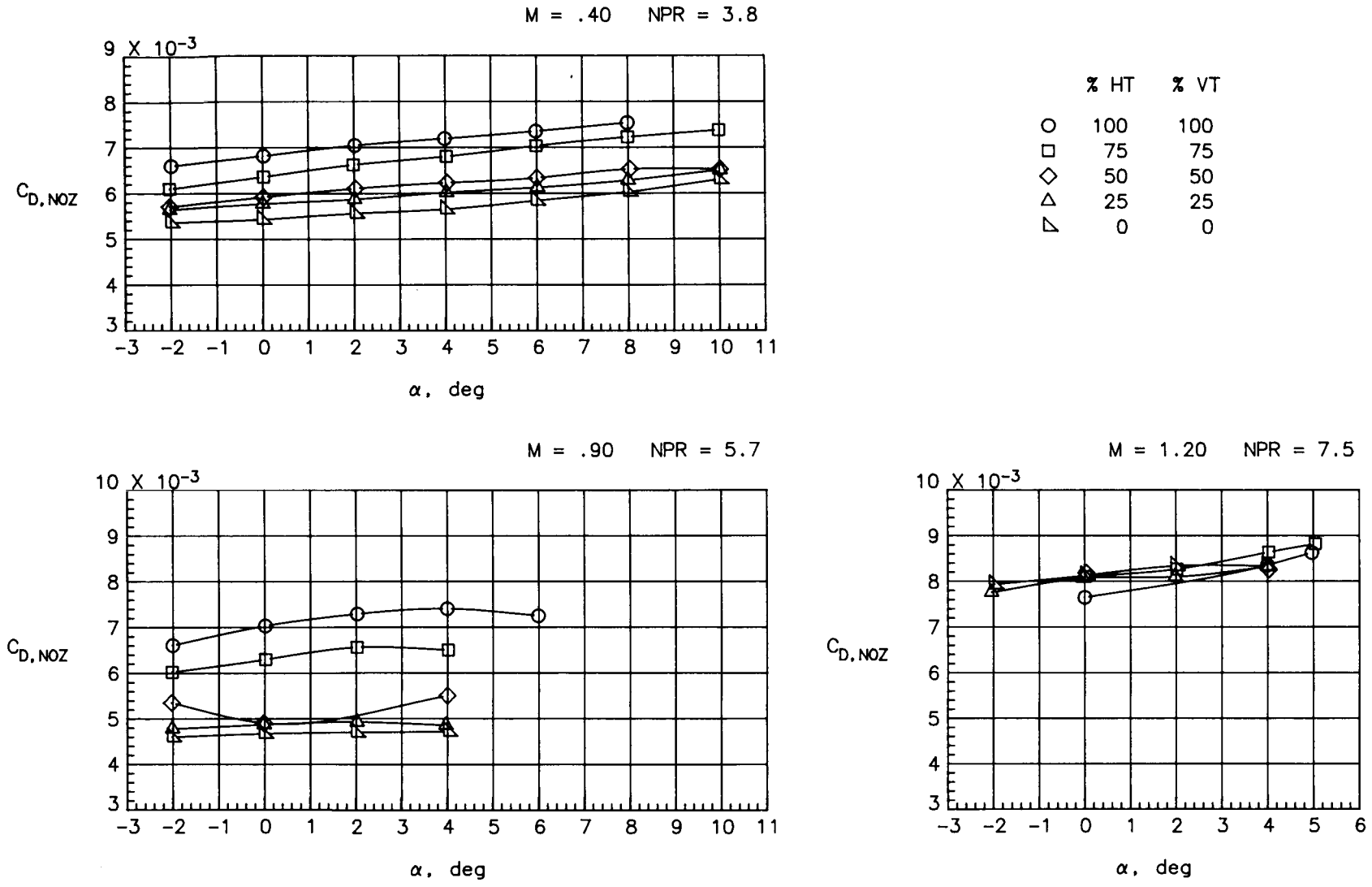

Figure 14. Effects of horizontal- and vertical-tail size on nozzle drag coefficient.

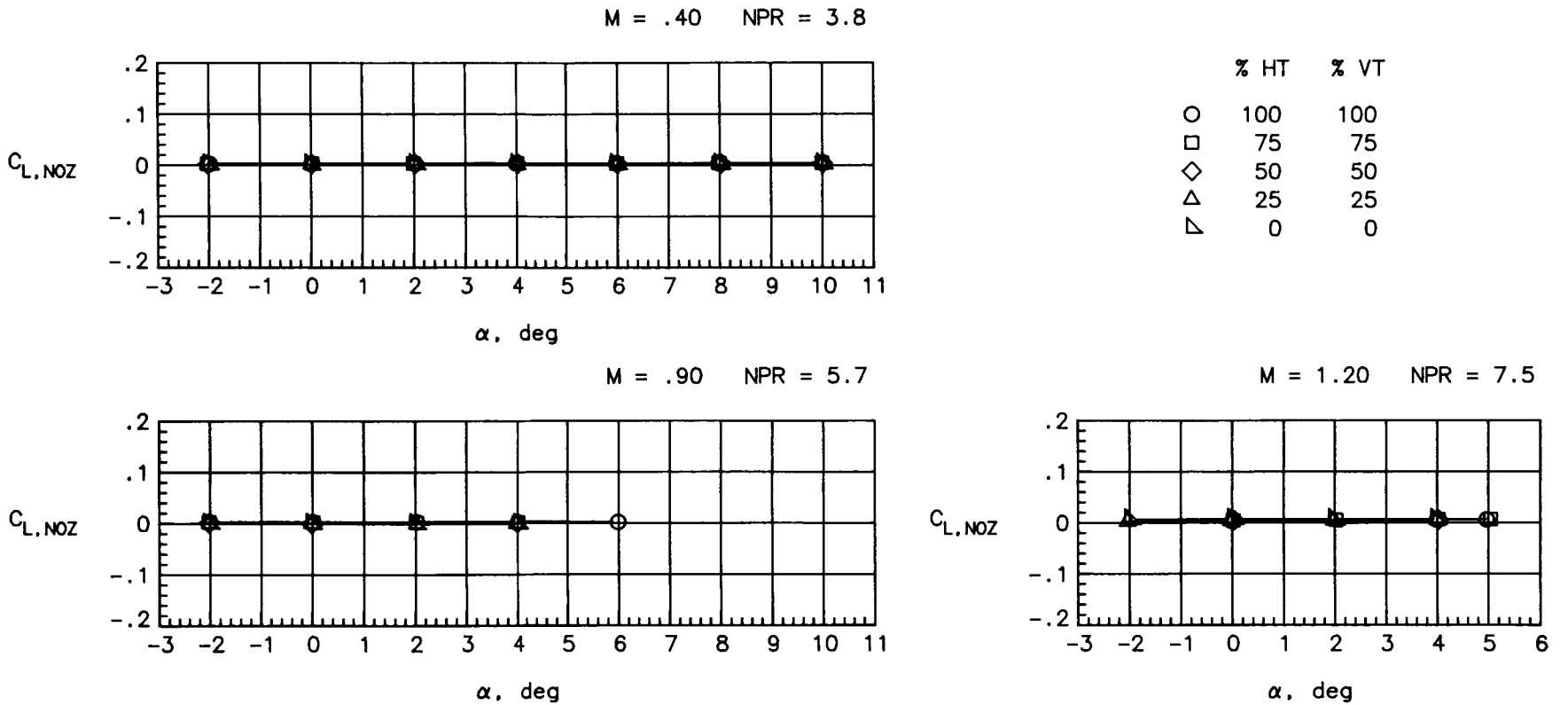

Figure 15. Effects of horizontal- and vertical-tail size on nozzle lift coefficient.

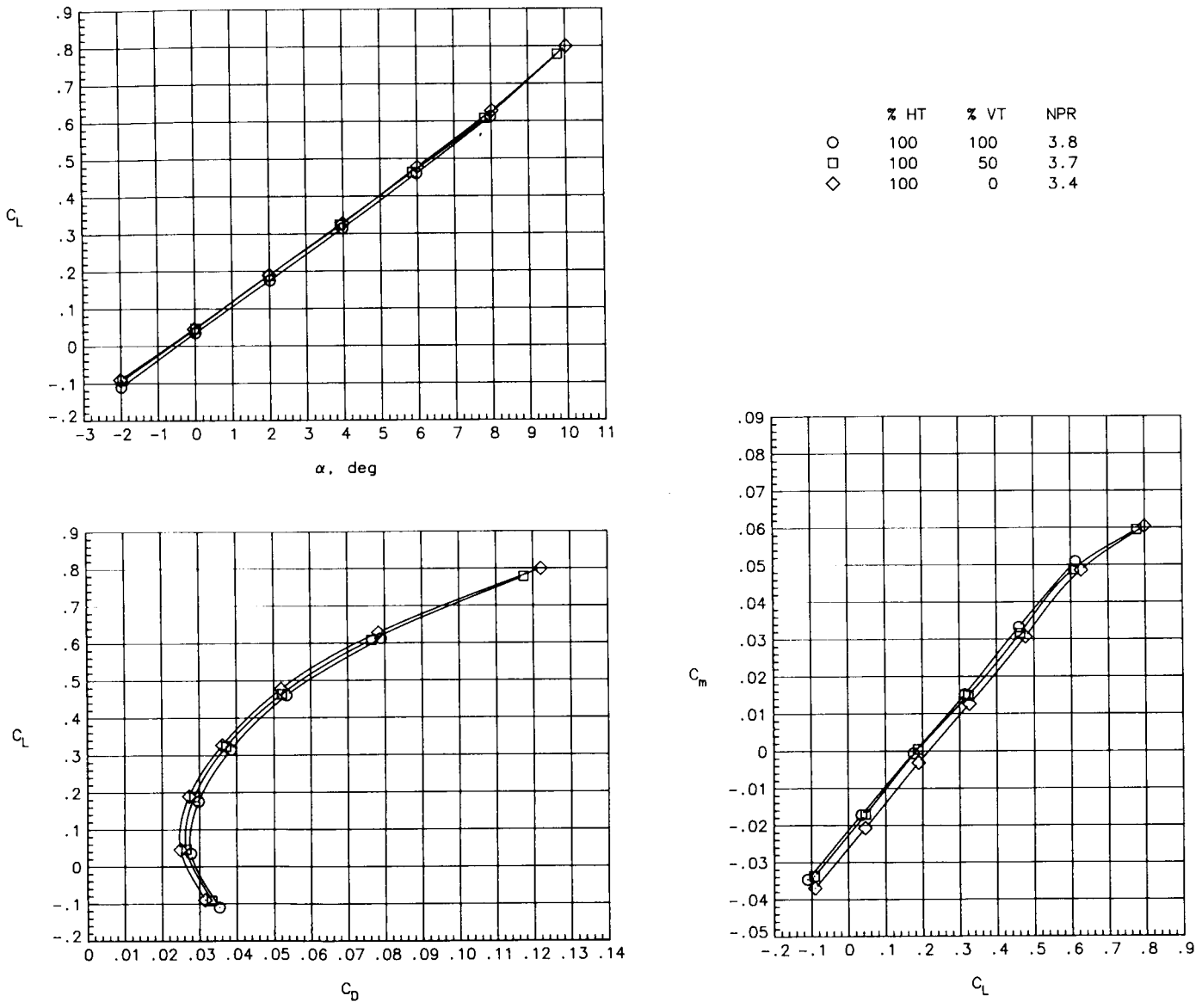

(a) $M = 0.40$.

Figure 16. Effects of vertical-tail size on longitudinal aerodynamic characteristics.

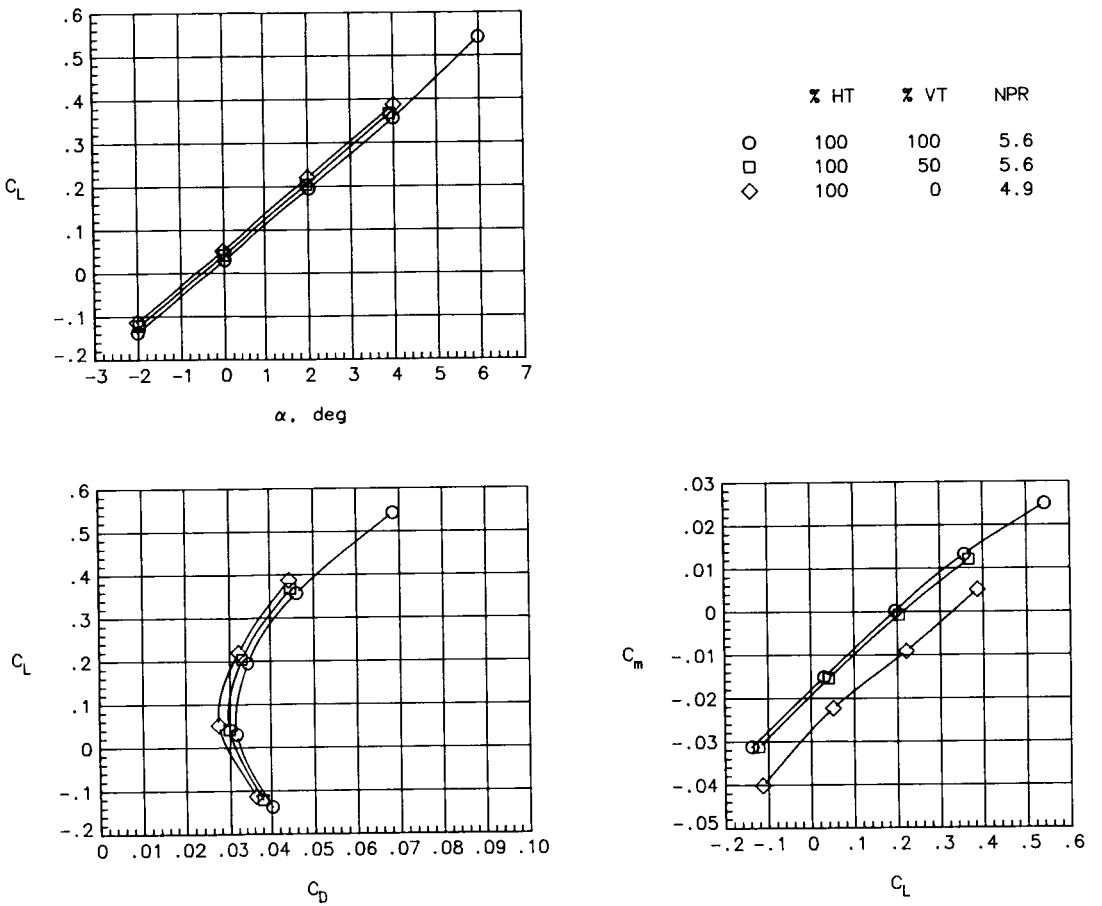

(b) $M = 0.90$.

Figure 16. Continued.

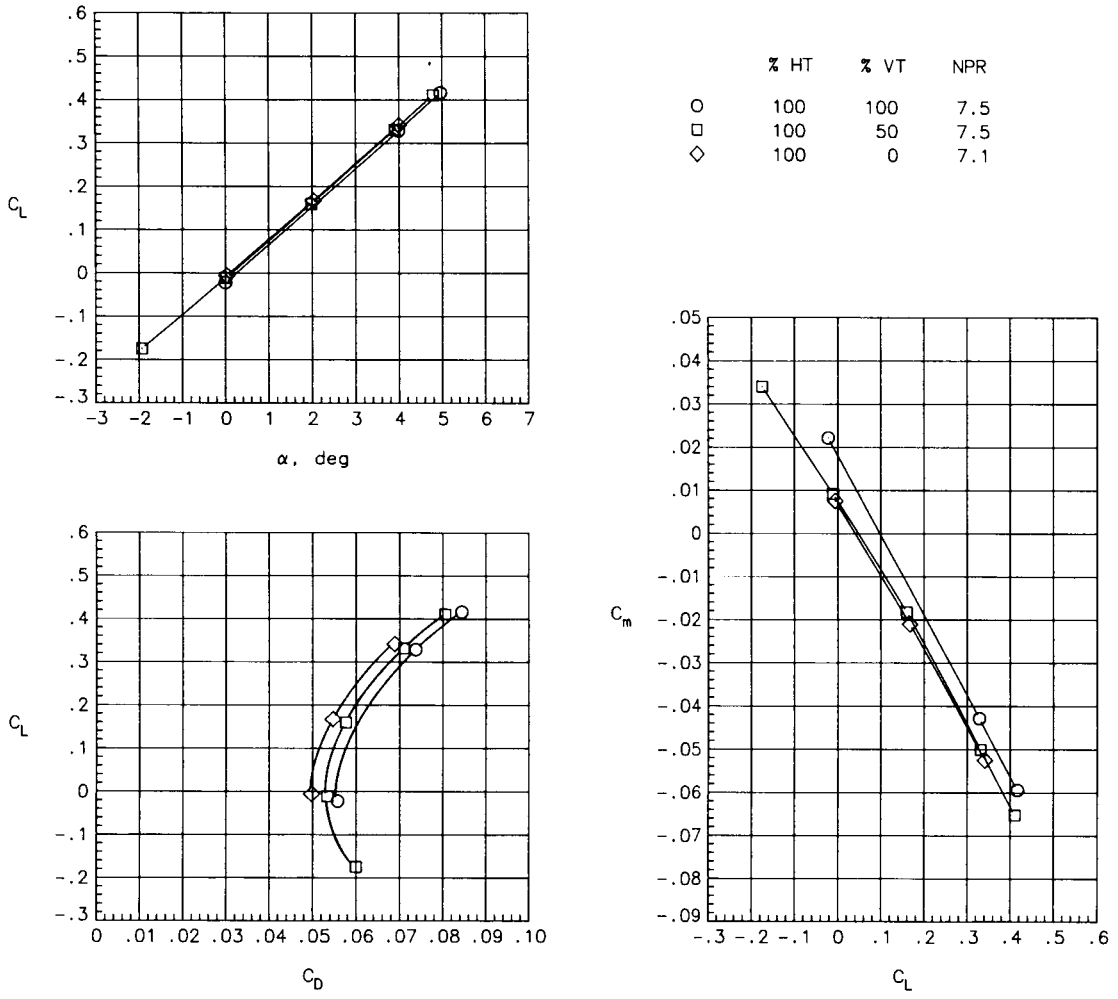

(c) $M = 1.20$.

Figure 16. Concluded.

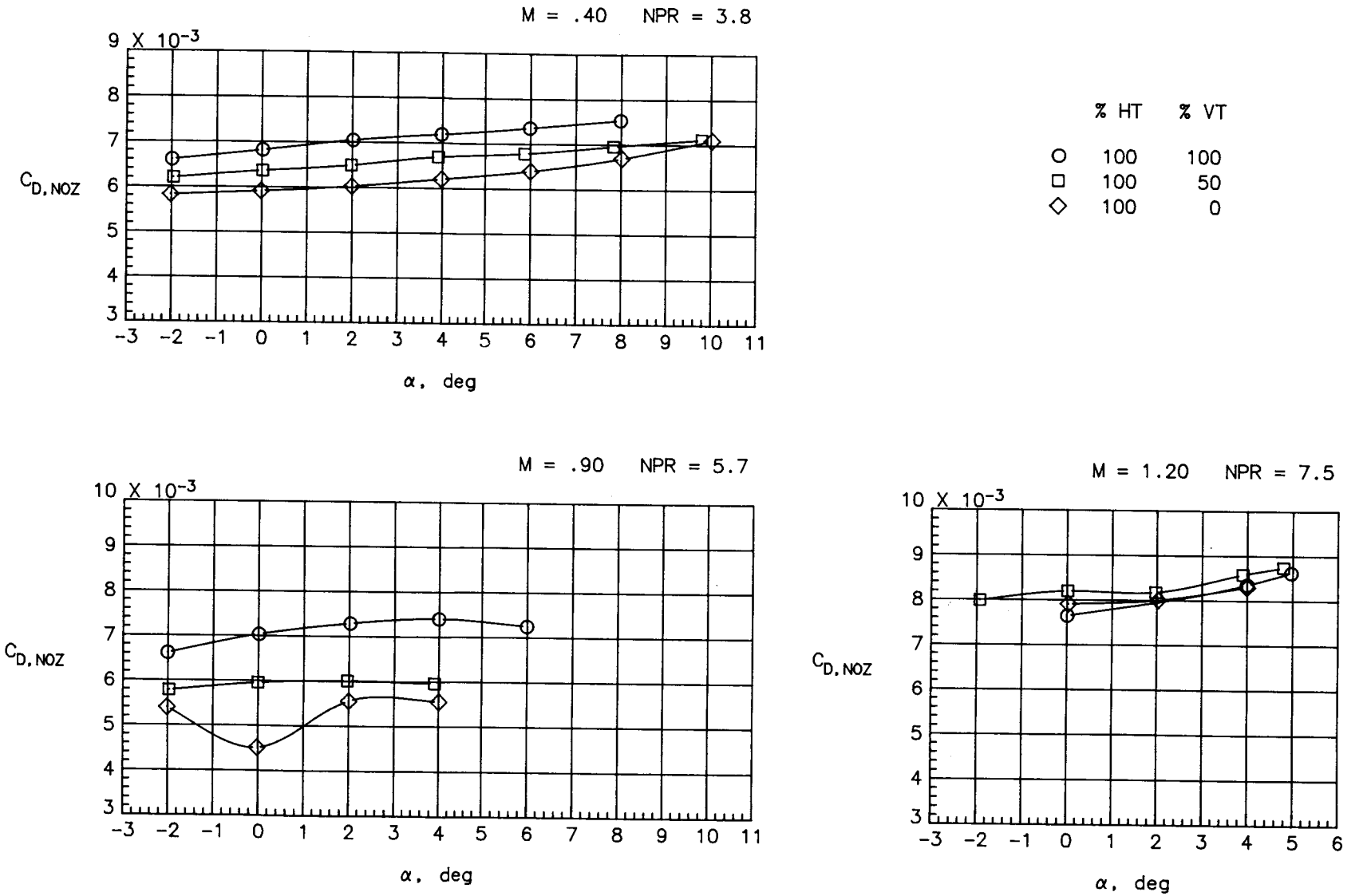

Figure 17. Effects of vertical-tail size on nozzle drag coefficient.

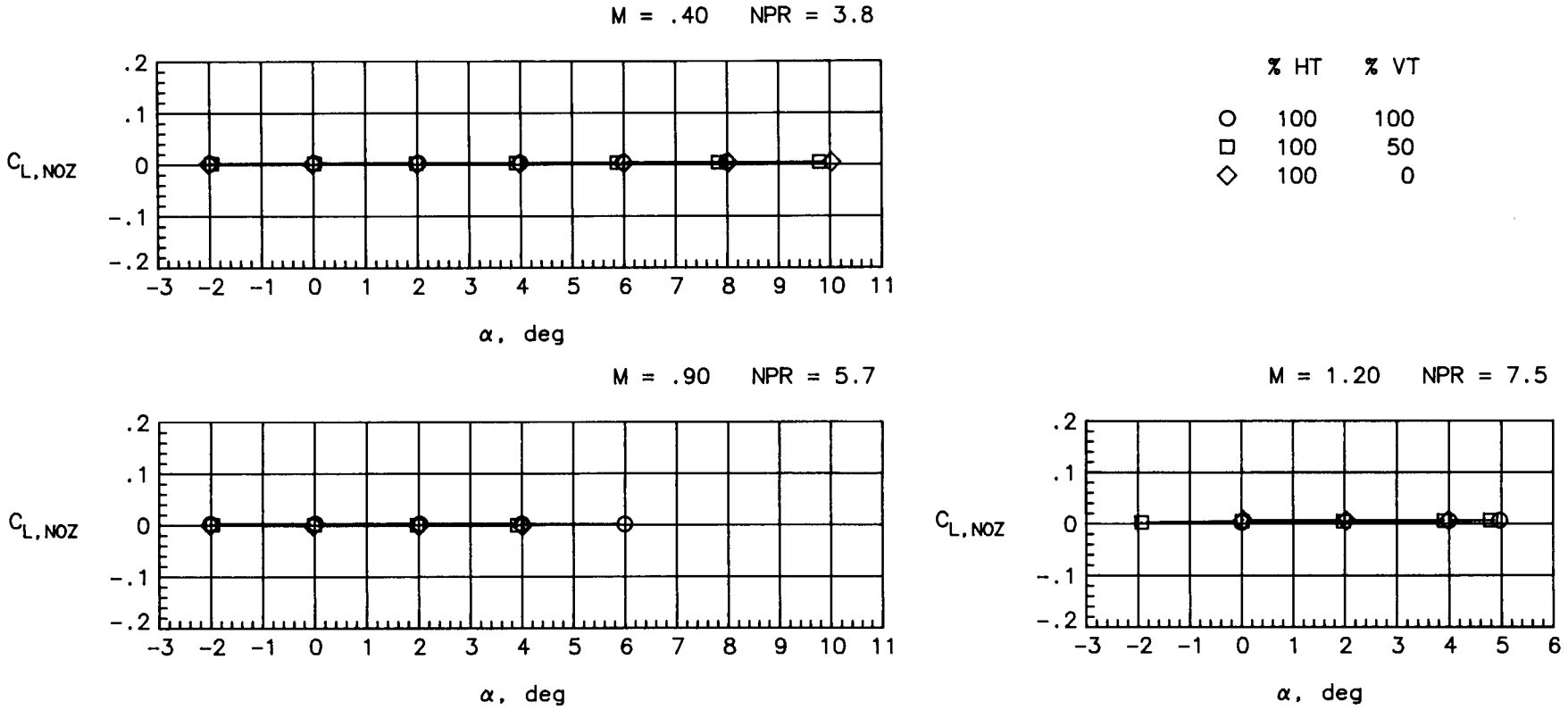

Figure 18. Effects of vertical-tail size on nozzle lift coefficient.

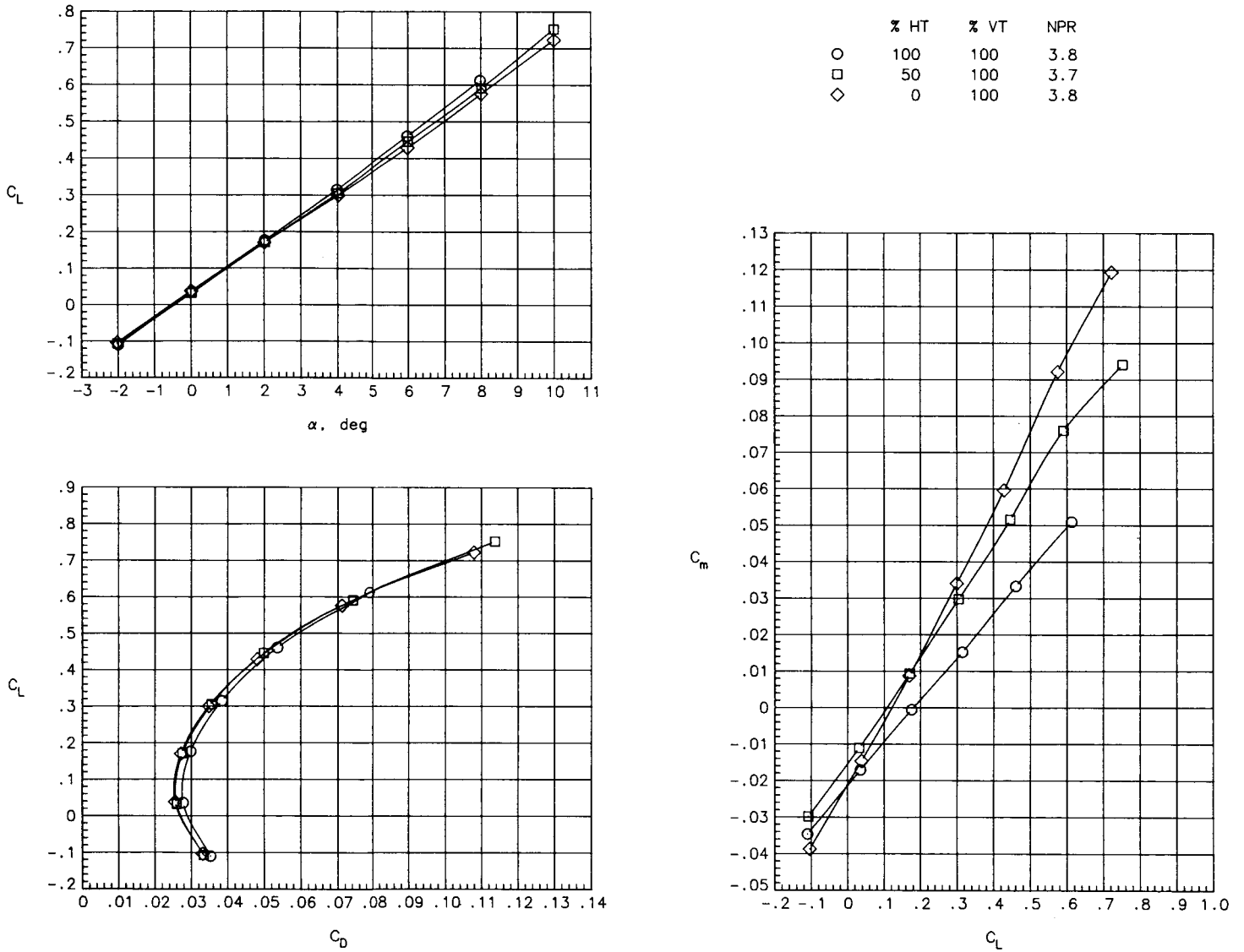

(a) $M = 0.40$.

Figure 19. Effects of horizontal-tail size on longitudinal aerodynamic characteristics.

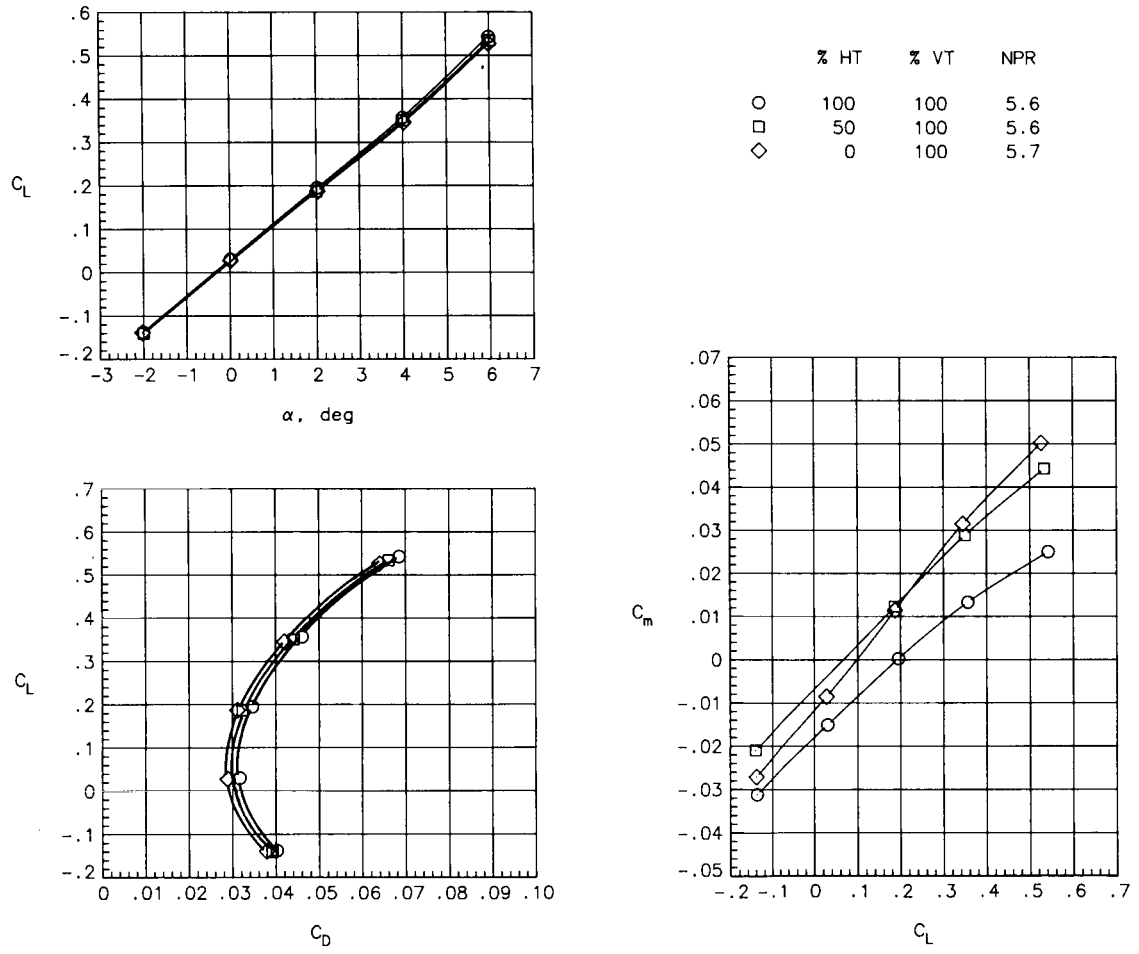

(b) $M = 0.90$.

Figure 19. Continued.

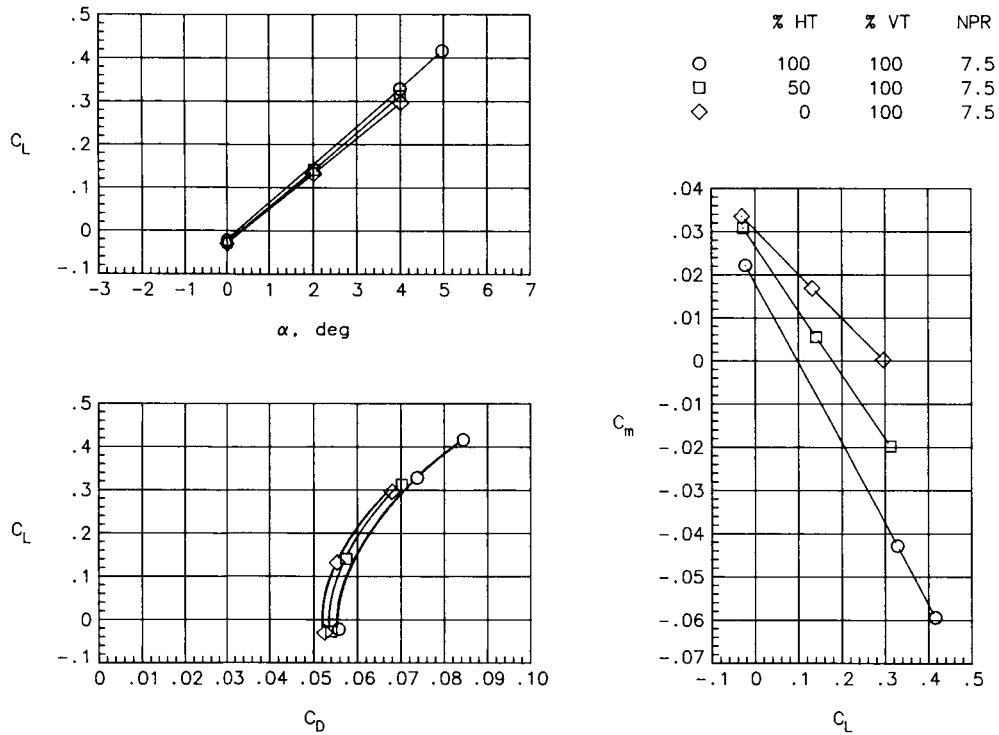

(c) $M = 1.20$.

Figure 19. Concluded.

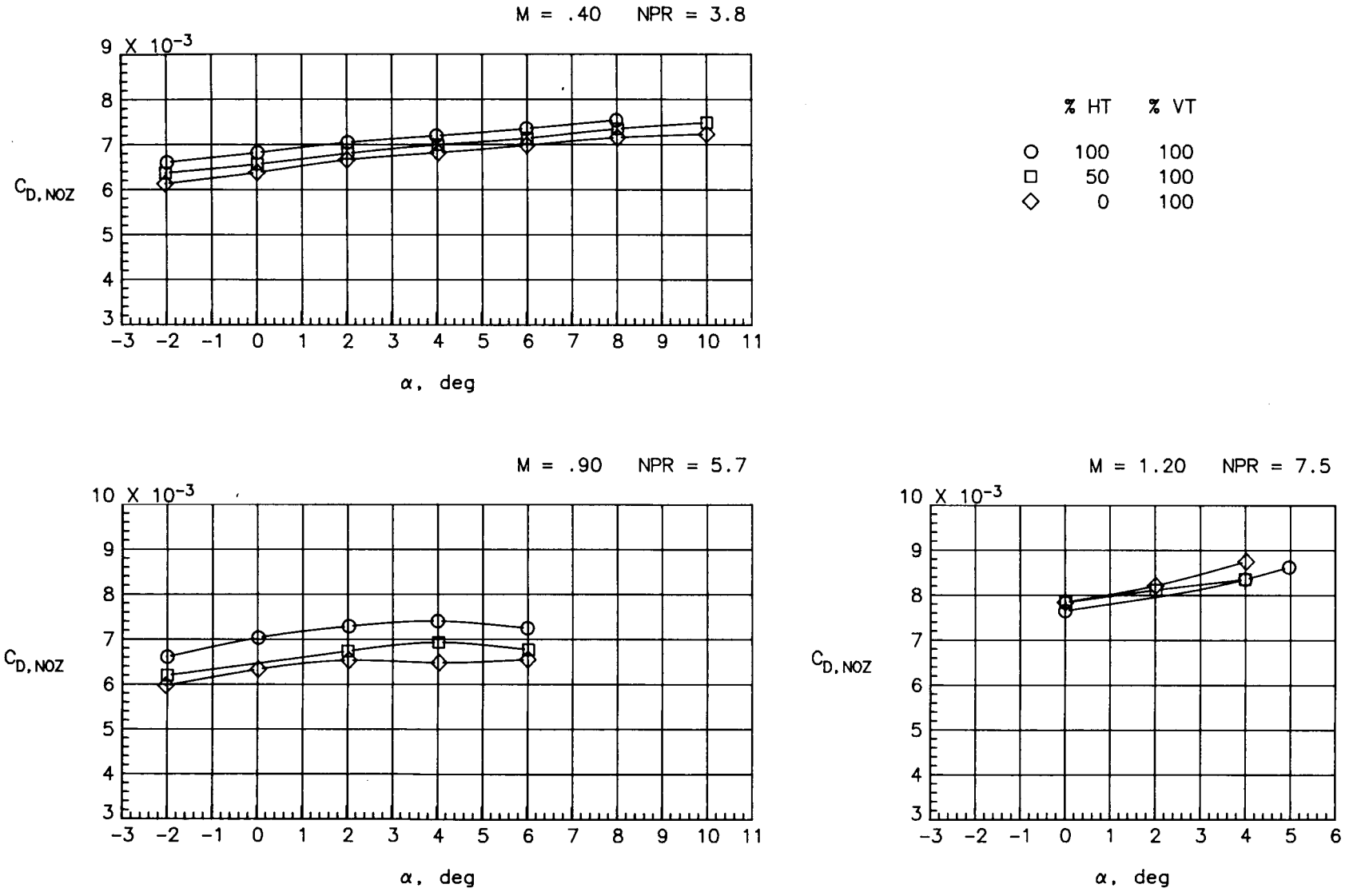

Figure 20. Effects of horizontal-tail size on nozzle drag coefficient.

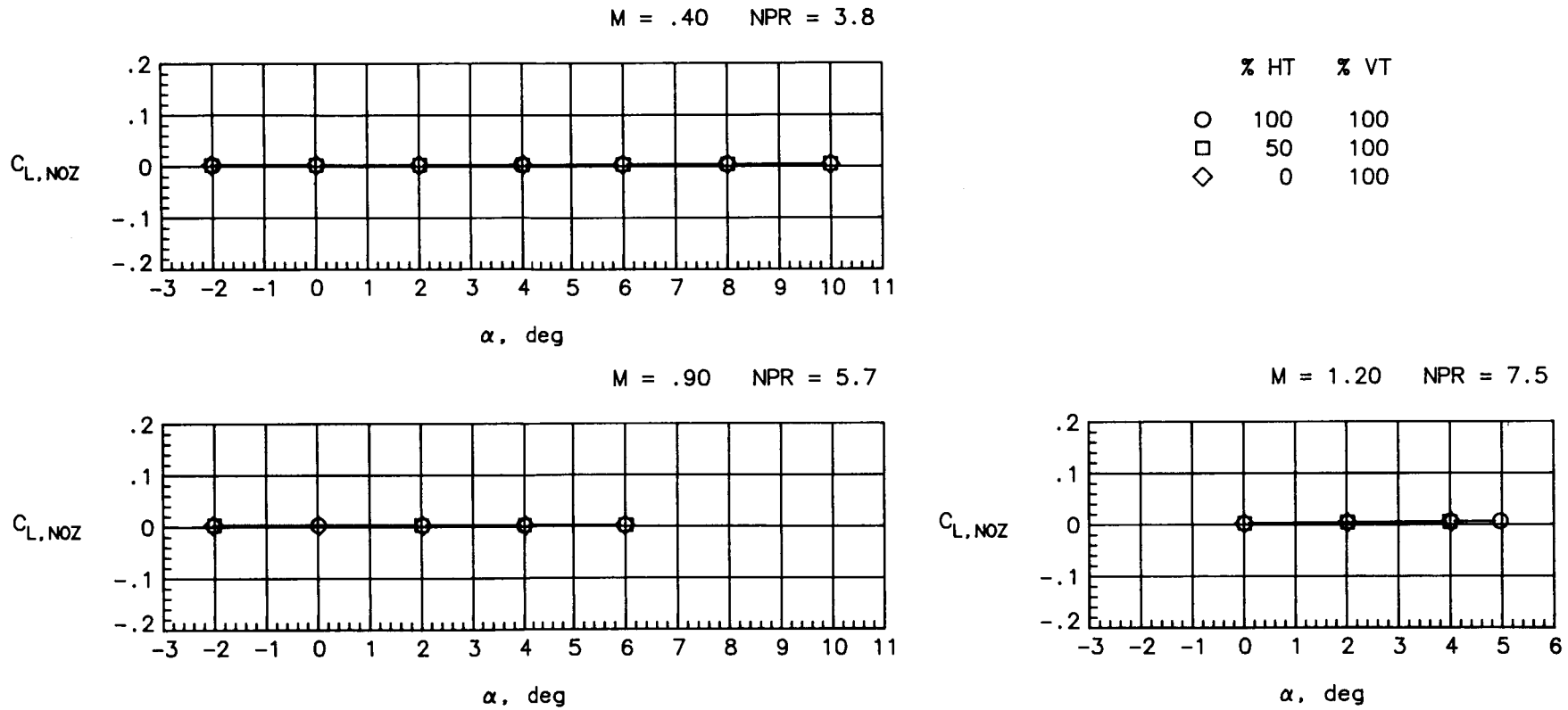

Figure 21. Effects of horizontal-tail size on nozzle lift coefficient.

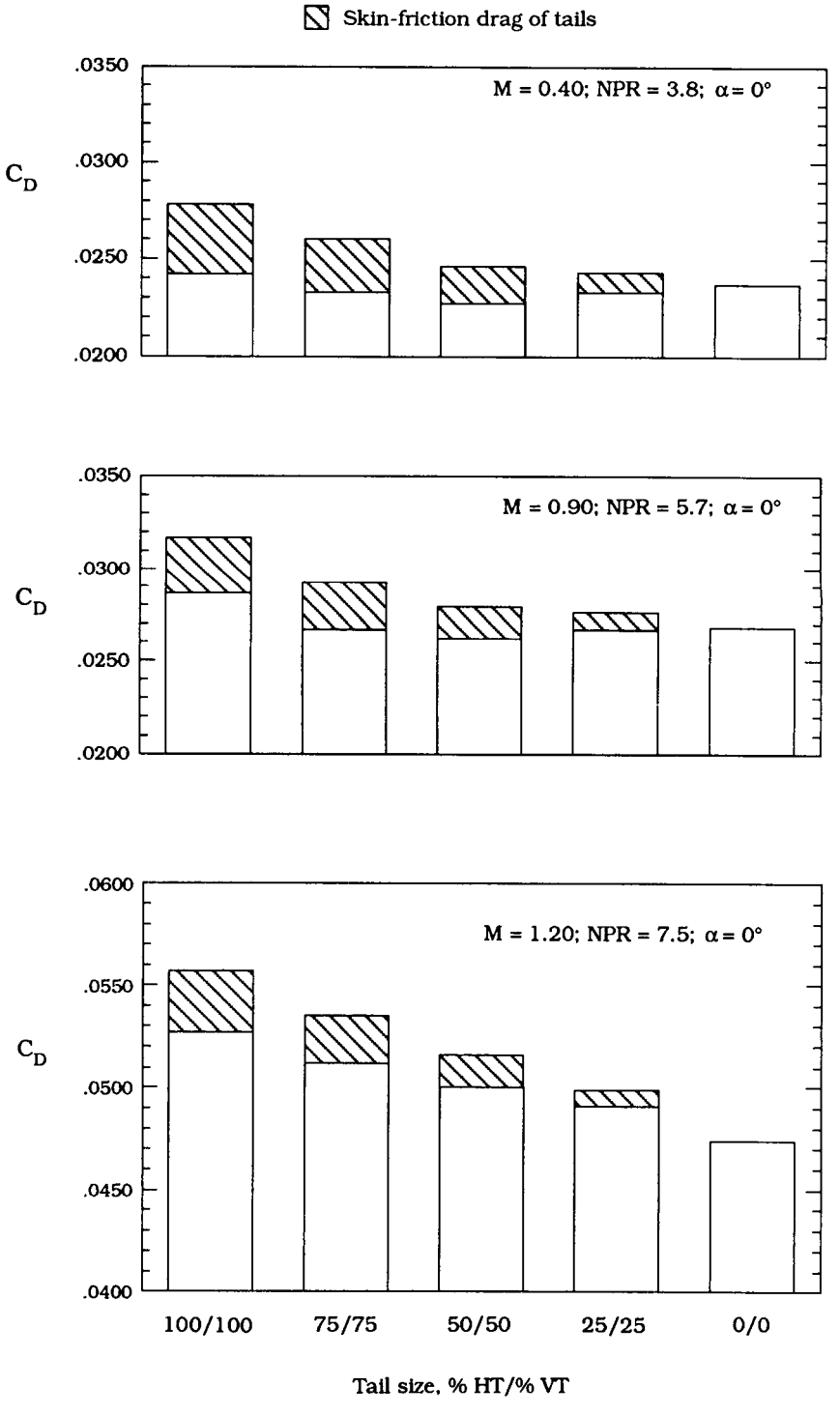

Figure 22. Effects of horizontal- and vertical-tail size on total drag coefficient.

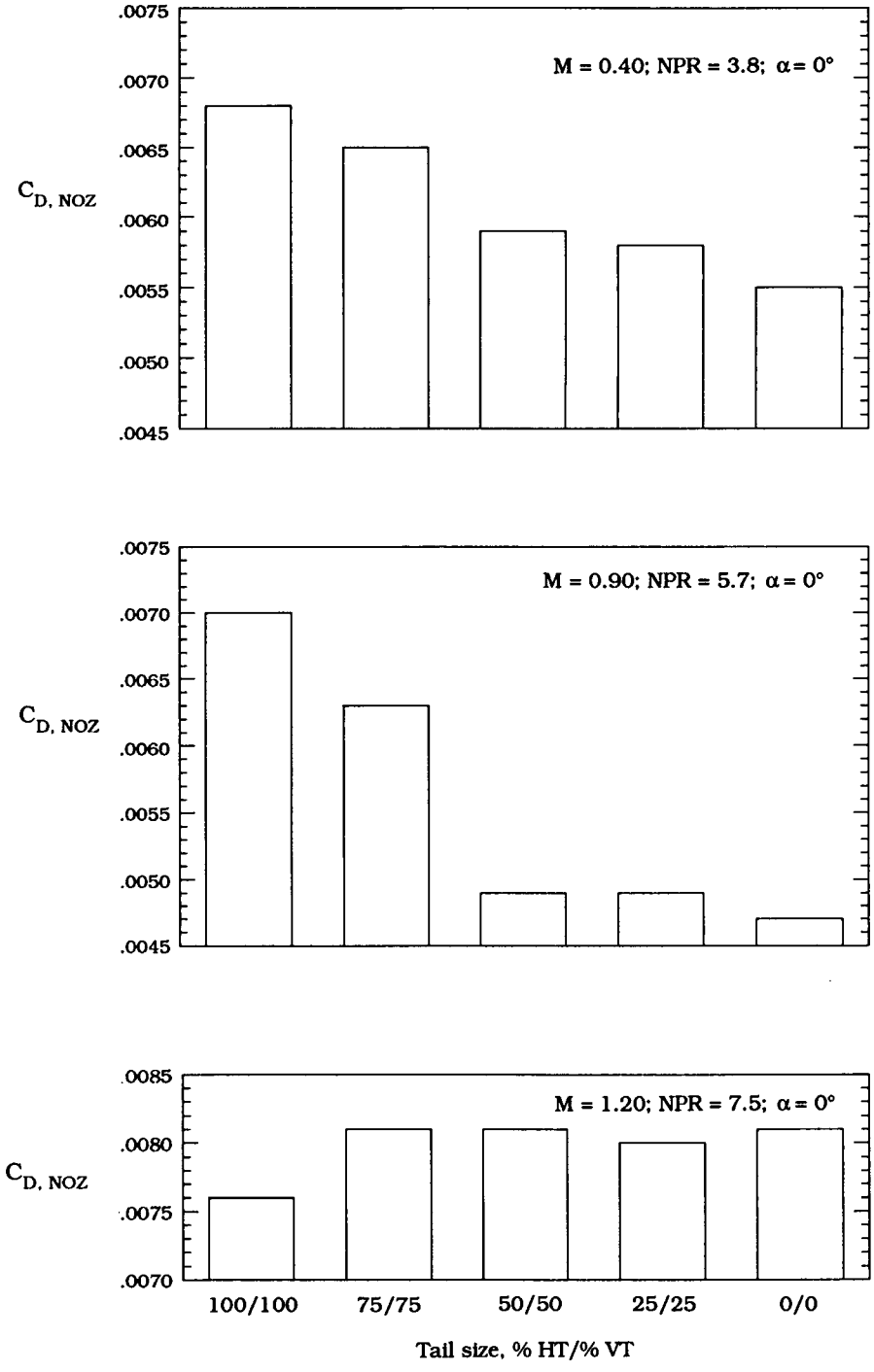

Figure 23. Effects of horizontal- and vertical-tail size on nozzle drag coefficient.

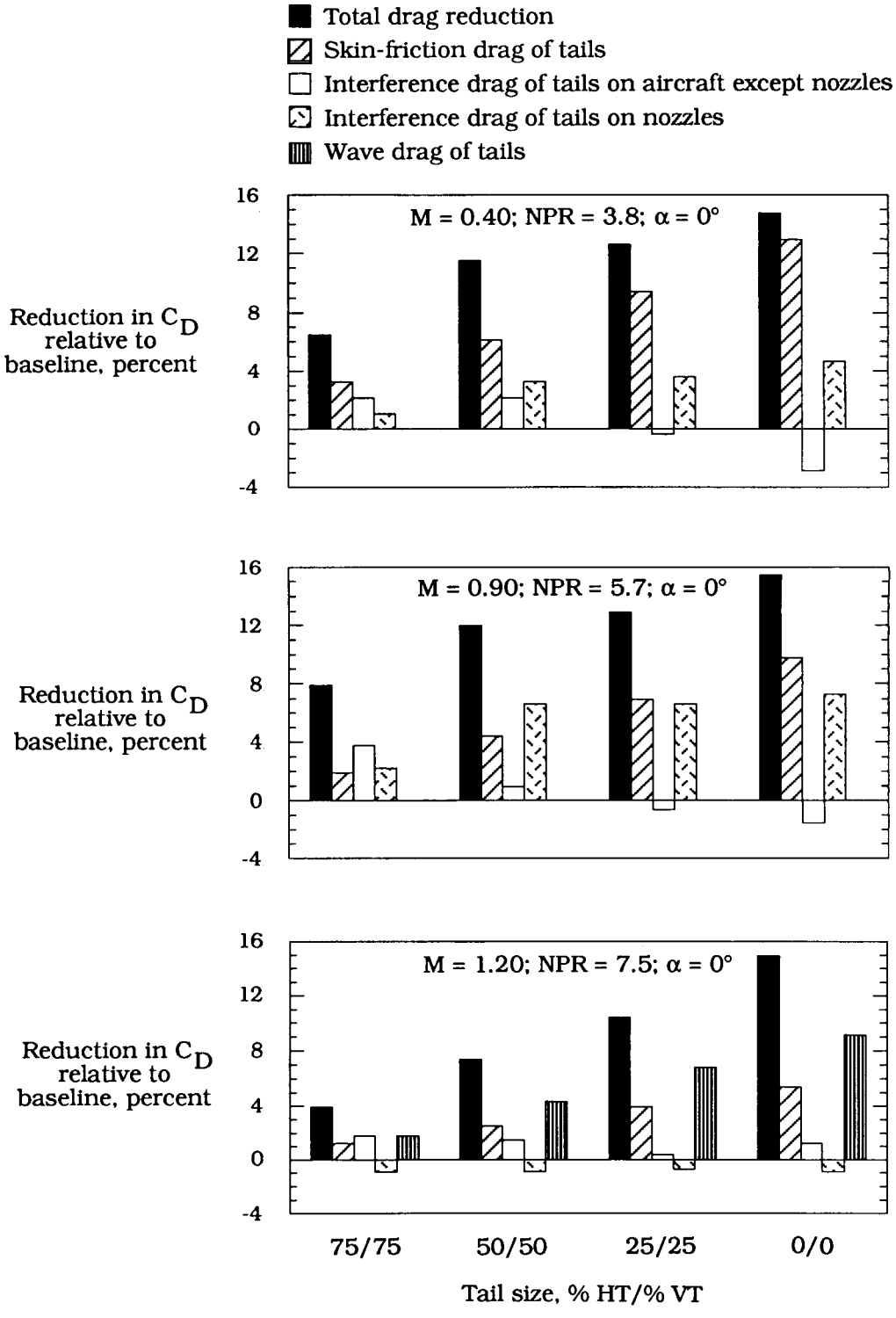

Figure 24. Effects of horizontal- and vertical-tail size on total drag reduction and its components.

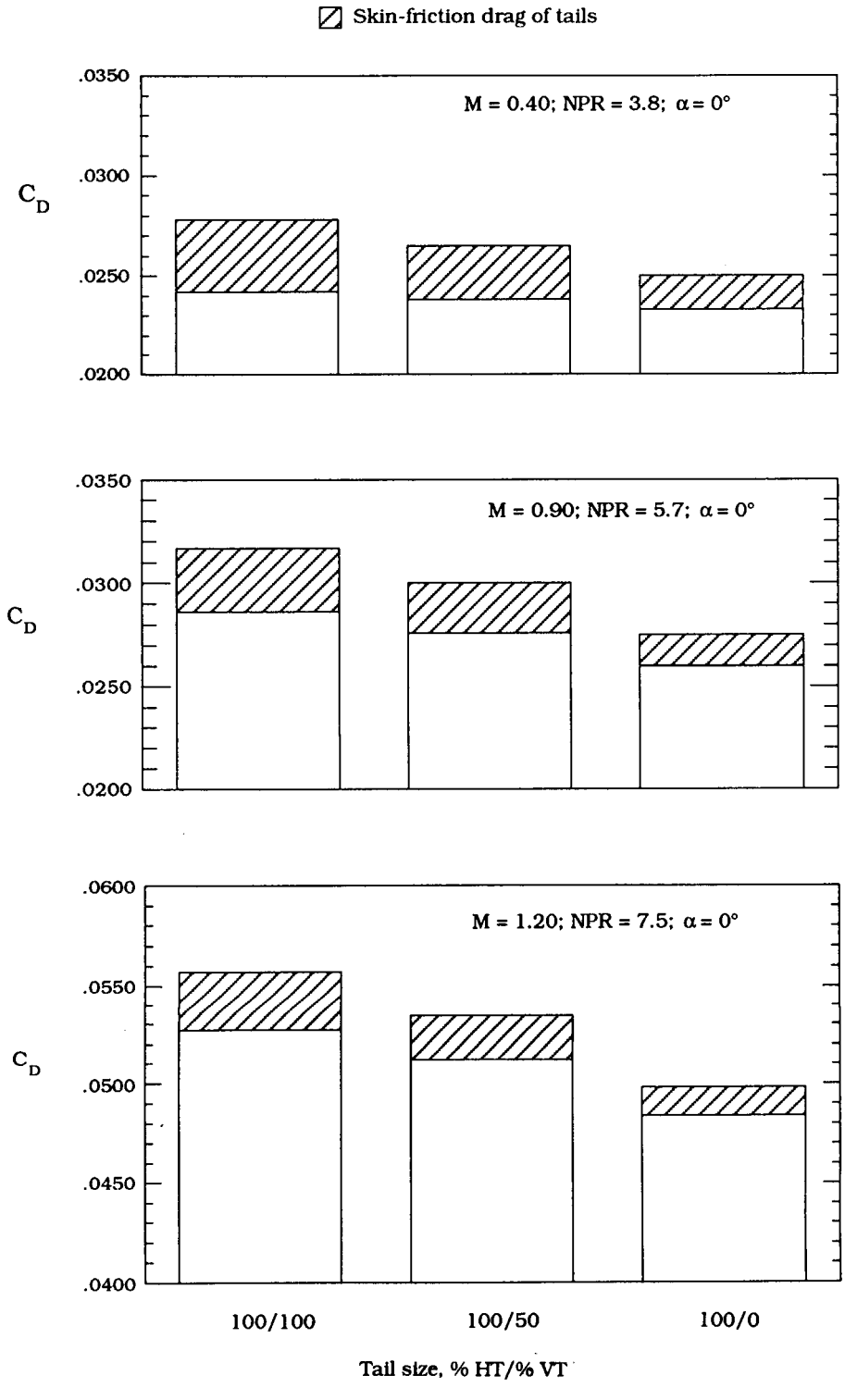

Figure 25. Effects of vertical-tail size on total drag coefficient.

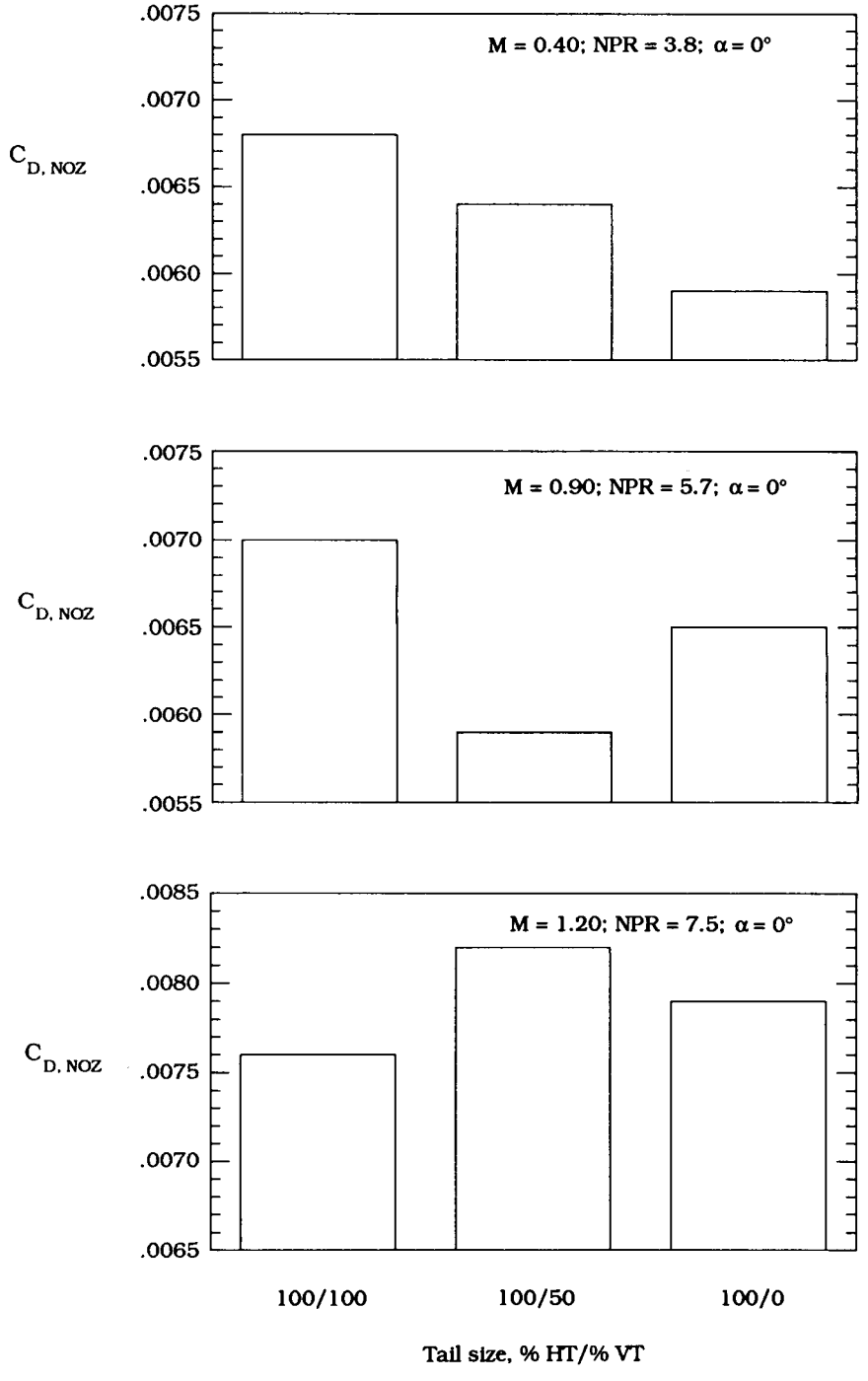

Figure 26. Effects of vertical-tail size on nozzle drag coefficient.

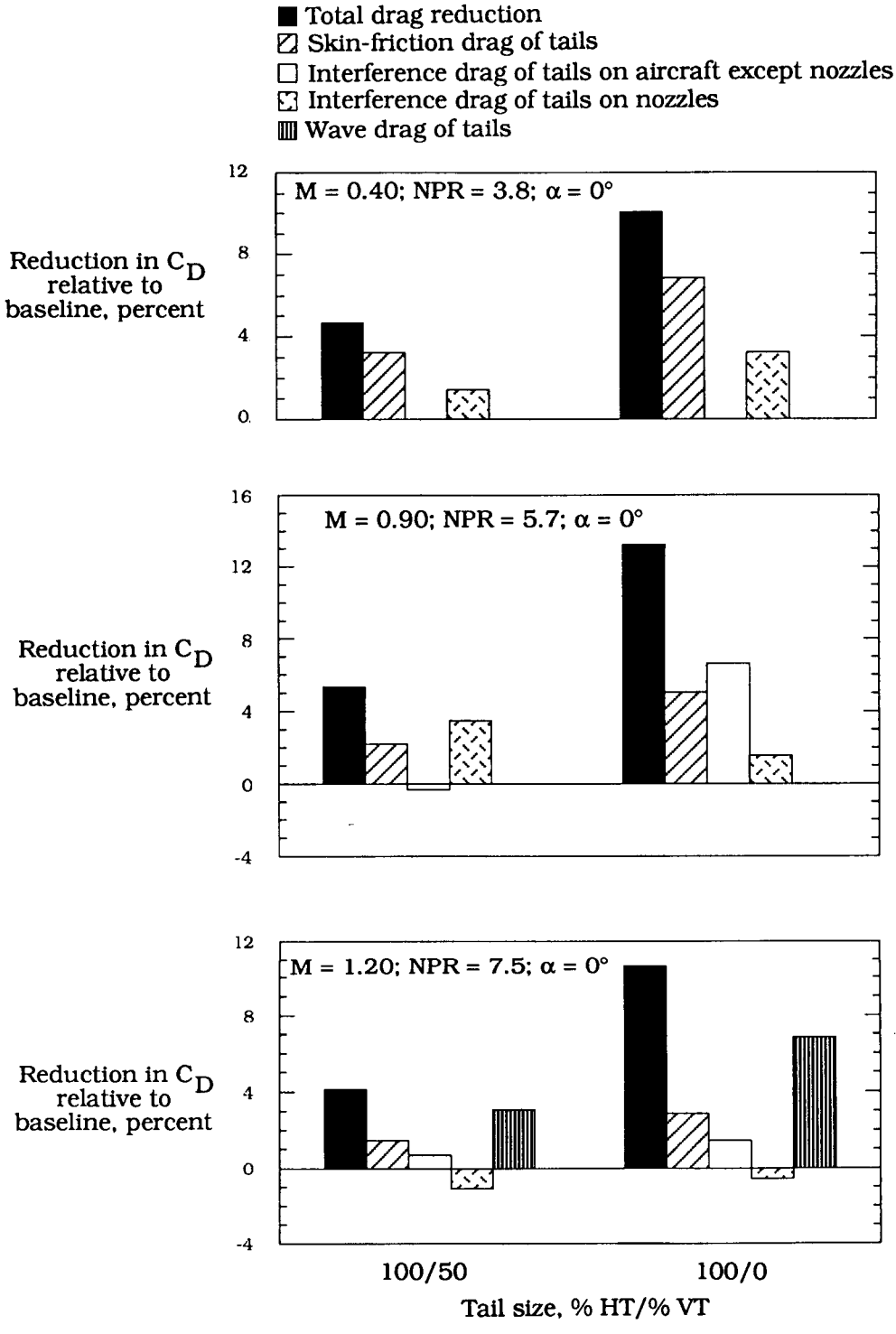

Figure 27. Effects of vertical-tail size on total drag reduction and its components.

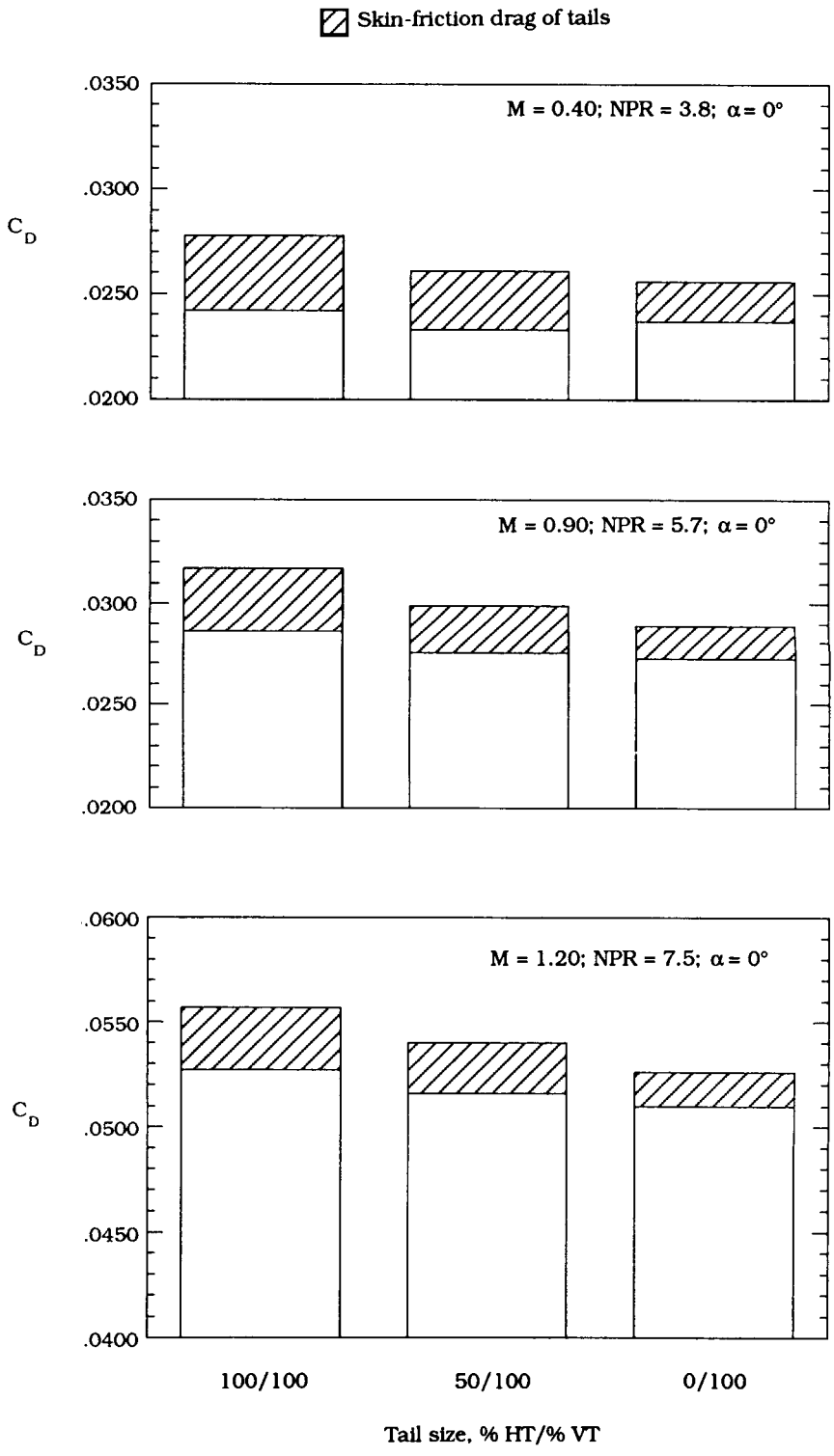

Figure 28. Effects of horizontal-tail size on total drag coefficient.

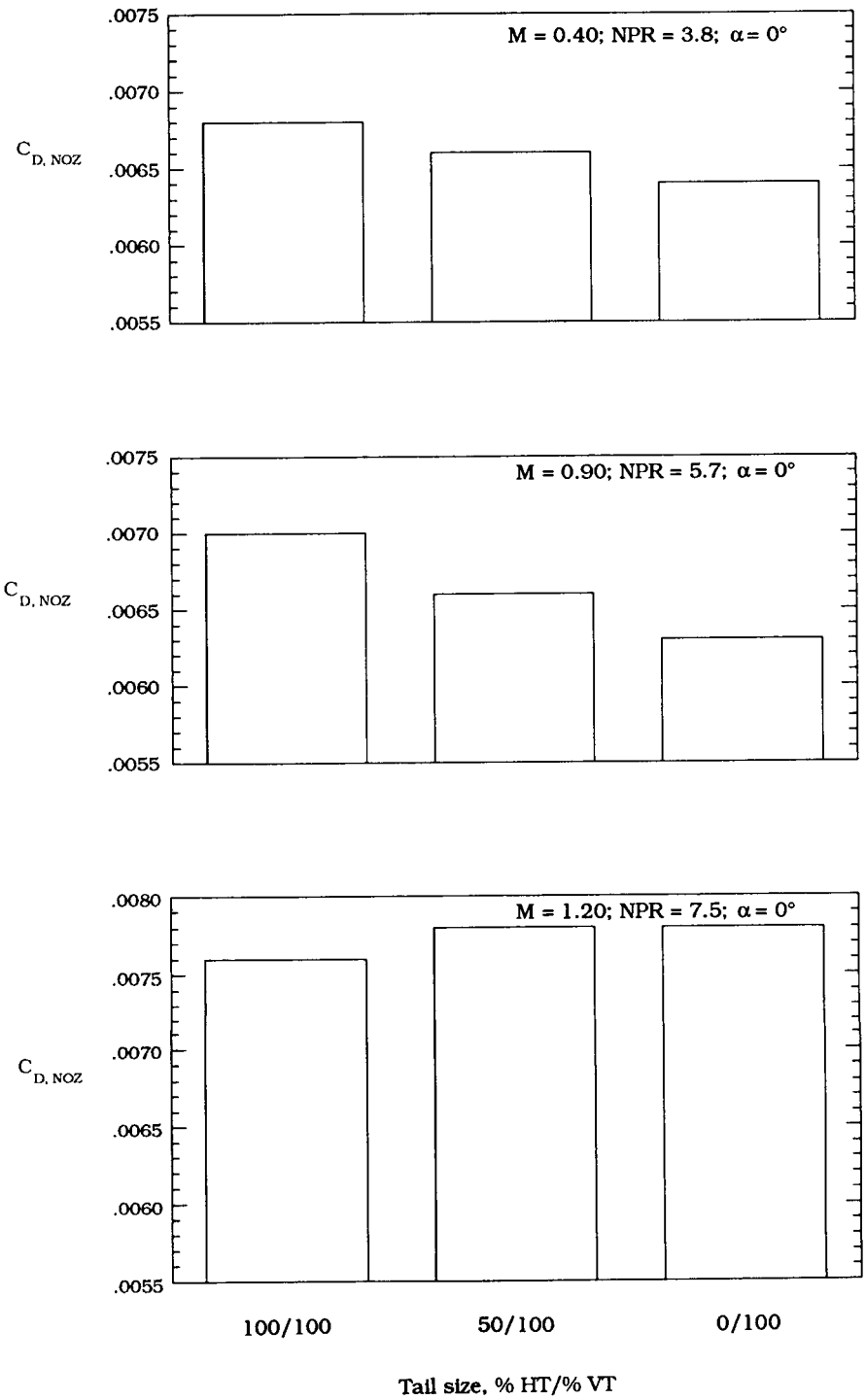

Figure 29. Effects of horizontal-tail size on nozzle drag coefficient.

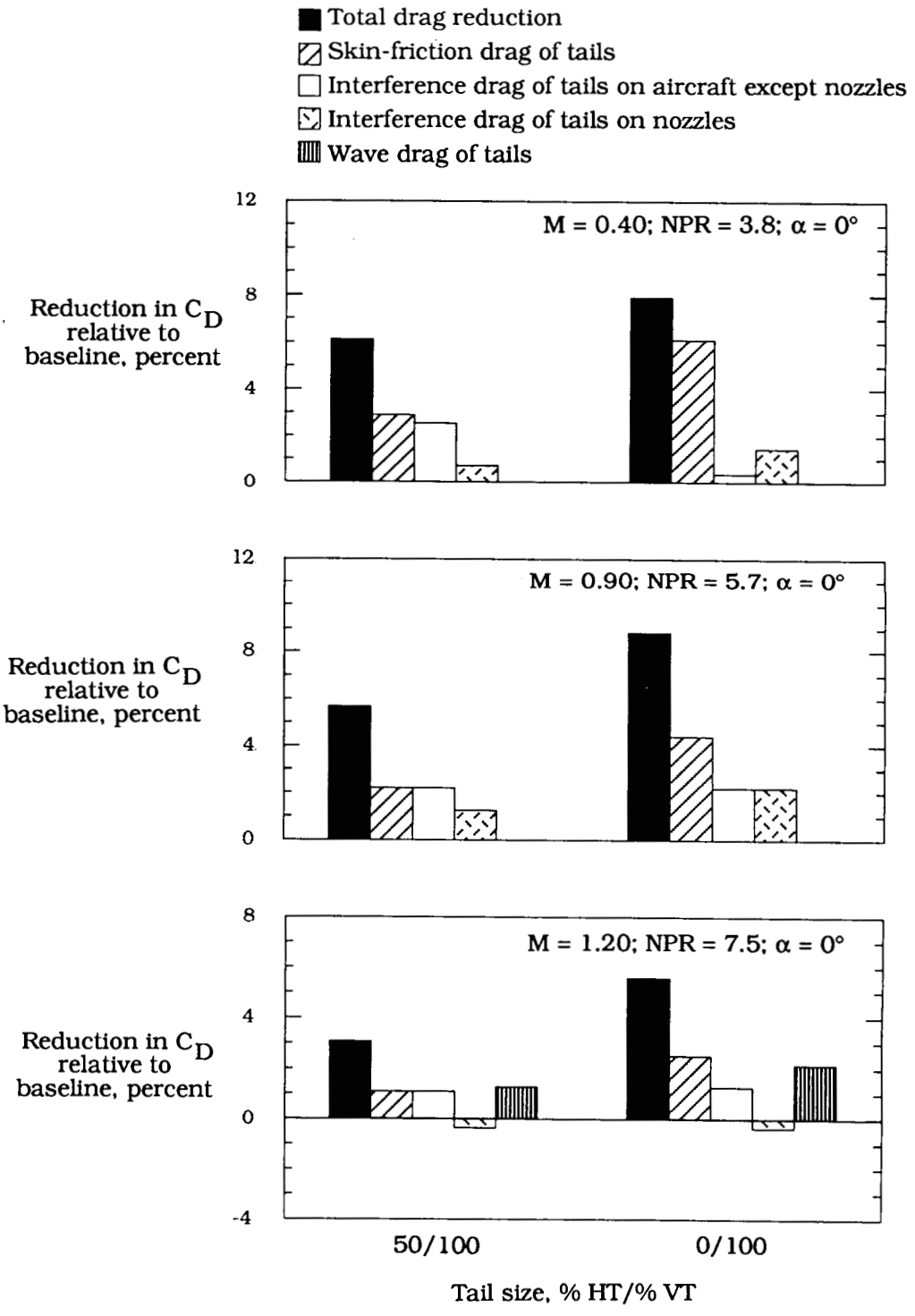

Figure 30. Effects of horizontal-tail size on total drag reduction and its components.

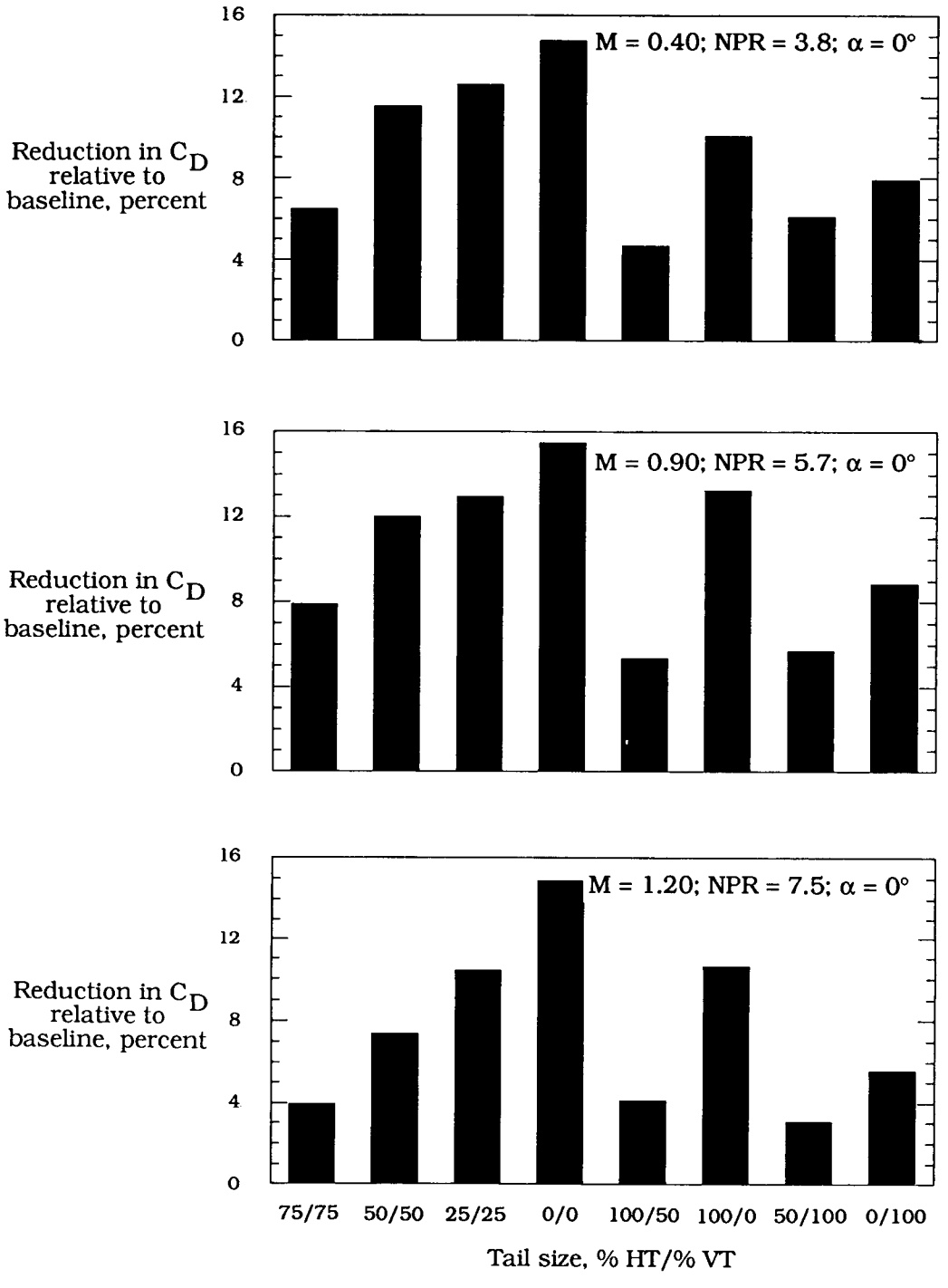

Figure 31. Summary of effects of horizontal- and/or vertical-tail size reductions on total drag reduction.

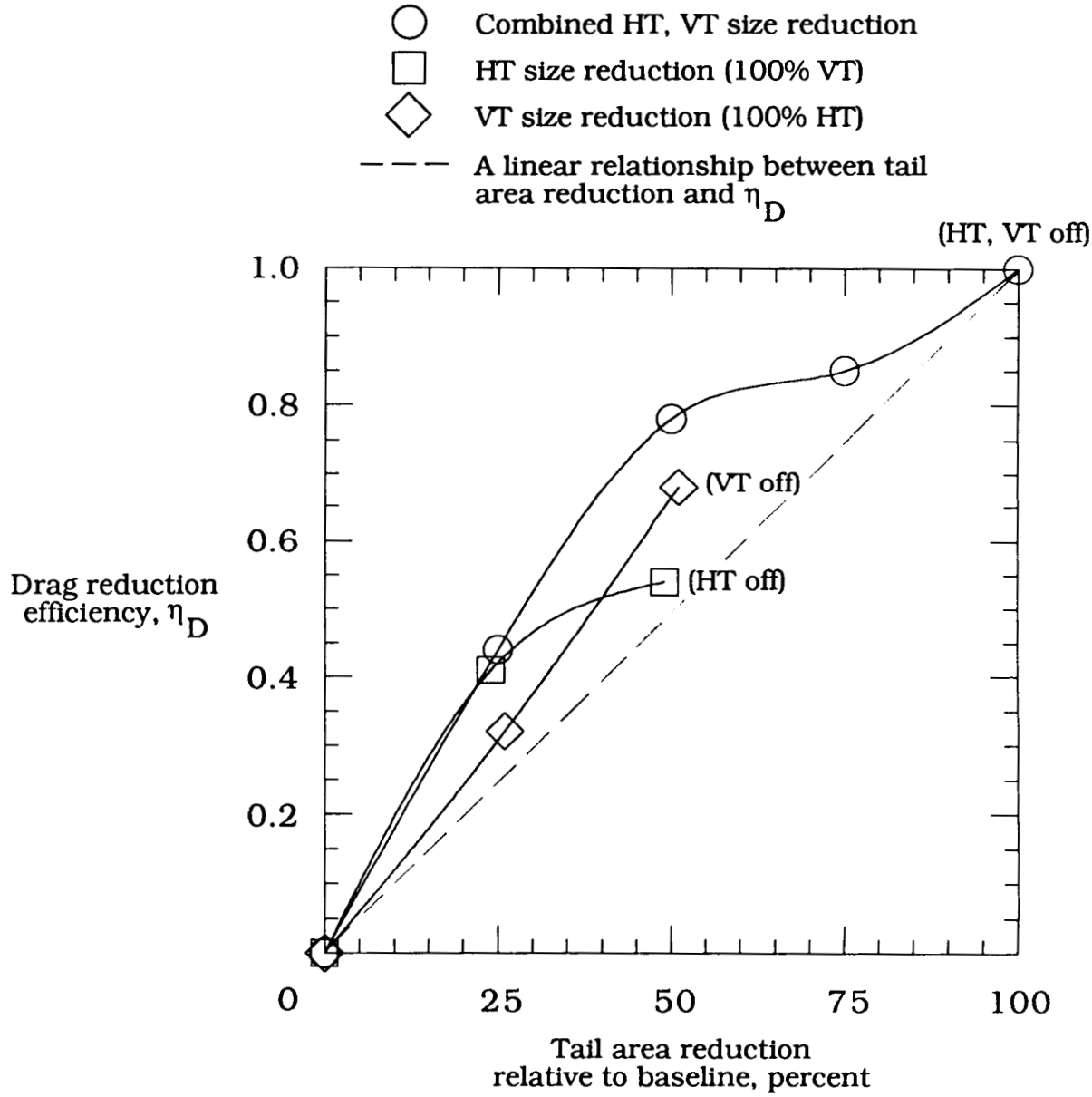

(a) $M = 0.40$; NPR = 3.8; $\alpha = 0°$.

Figure 32. Summary of drag reduction efficiency of each horizontal- and vertical-tail combination.

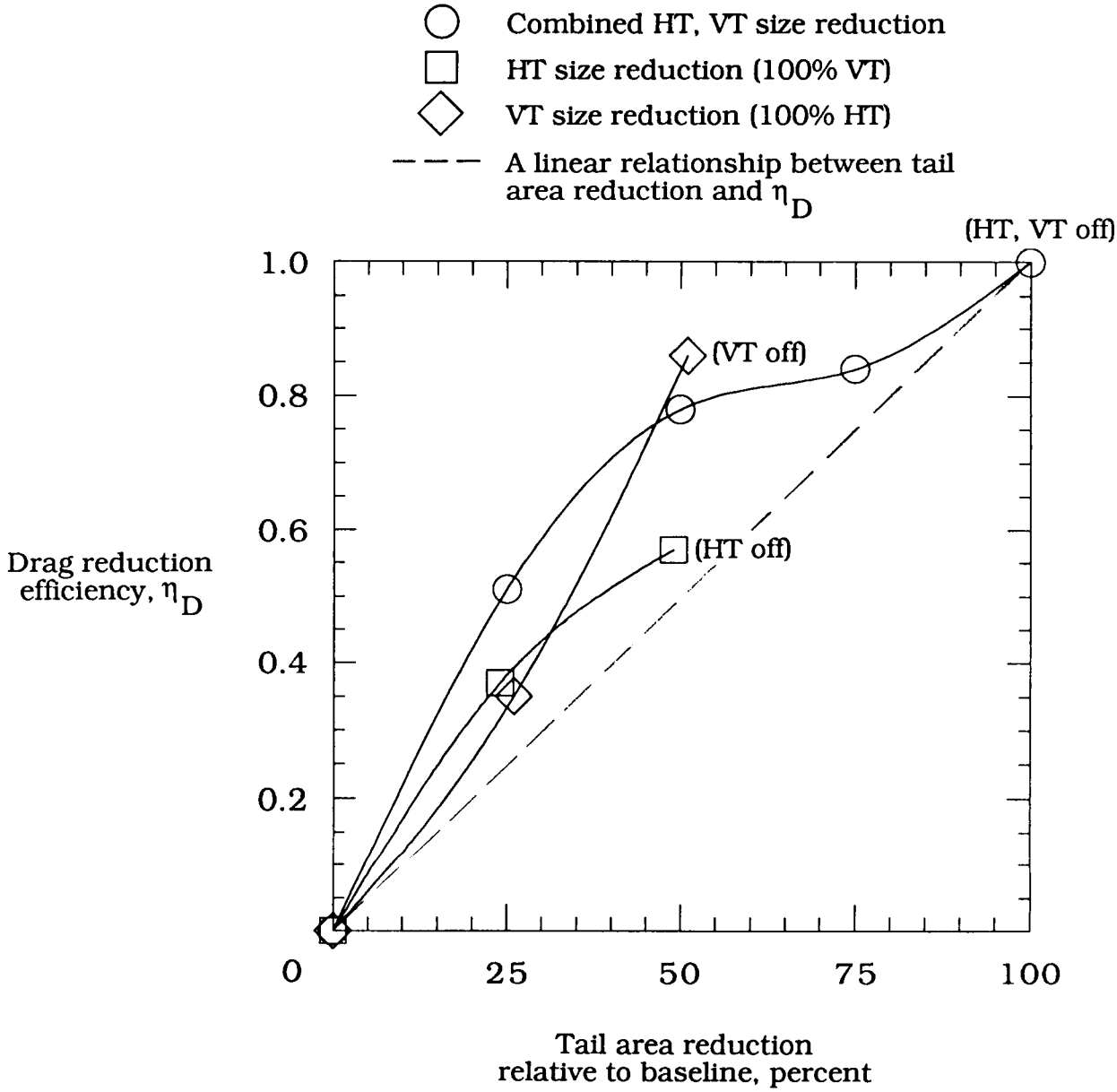

(b) $M = 0.90$; NPR = 5.7; $\alpha = 0°$.

Figure 32. Continued.

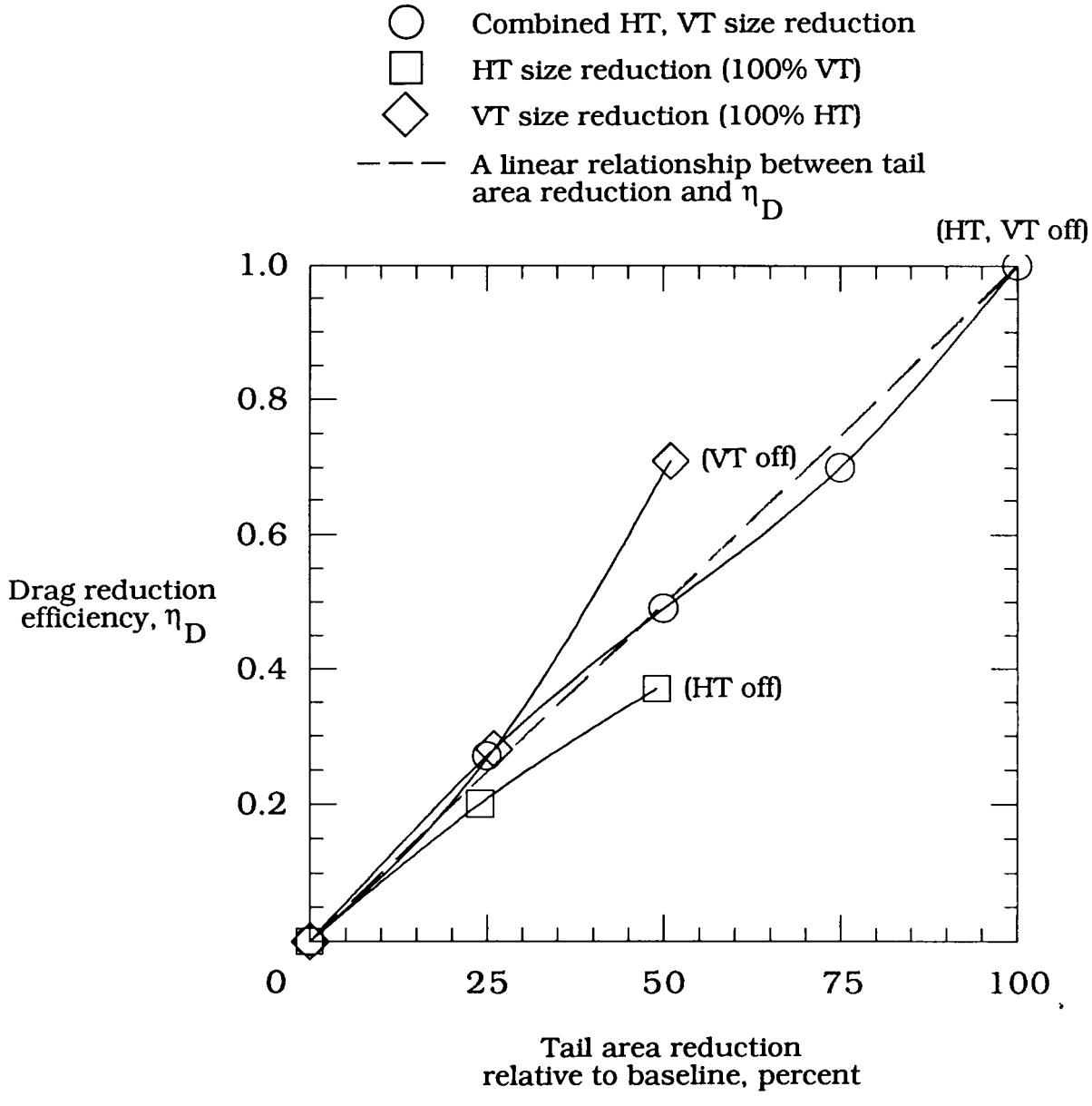

(c) $M = 1.20$; NPR = 7.5; $\alpha = 0°$.

Figure 32. Concluded.

NASA
National Aeronautics and Space Administration

Report Documentation Page

1. Report No.	2. Government Accession No.	3. Recipient's Catalog No.
NASA TP-3036		

4. Title and Subtitle	5. Report Date
Effect of Tail Size Reductions on Longitudinal Aerodynamic Characteristics of a Three-Surface F-15 Model With Nonaxisymmetric Nozzles	August 1990
	6. Performing Organization Code
7. Author(s)	8. Performing Organization Report No.
Mark C. Frassinelli and George T. Carson, Jr.	L-16800
9. Performing Organization Name and Address	10. Work Unit No.
NASA Langley Research Center Hampton, VA 23665-5225	505-62-71-01
	11. Contract or Grant No.
12. Sponsoring Agency Name and Address	13. Type of Report and Period Covered
National Aeronautics and Space Administration Washington, DC 20546-0001	Technical Paper
	14. Sponsoring Agency Code

15. Supplementary Notes

Mark C. Frassinelli: Detailed to NASA from Air Force Wright Research and Development Center, Wright-Patterson Air Force Base, Ohio.

George T. Carson, Jr.: Langley Research Center, Hampton, Virginia.

16. Abstract

An investigation was conducted in the Langley 16-Foot Transonic Tunnel to determine the effects of horizontal- and vertical-tail size reductions on the longitudinal aerodynamic characteristics of a modified F-15 model with canards and two-dimensional convergent-divergent nozzles. This study focused primarily on quantifying the drag decrease at low angles of attack produced by tail size reductions. The model was tested at Mach numbers of 0.40, 0.90, and 1.20 over an angle-of-attack range from $-2°$ to $10°$. The nozzle exhaust flow was simulated by using high-pressure air at nozzle pressure ratios from 1.0 (jet off) to 7.5. Data were obtained on the baseline configuration with and without tails and with reduced horizontal- and vertical-tail sizes that were 75, 50, and 25 percent of the baseline tail areas.

17. Key Words (Suggested by Authors(s))	18. Distribution Statement
Propulsion integration Tail size reduction Transonic aerodynamics	Unclassified—Unlimited Subject Category 02

19. Security Classif. (of this report)	20. Security Classif. (of this page)	21. No. of Pages	22. Price
Unclassified	Unclassified	57	A04

For sale by the National Technical Information Service, Springfield, Virginia 22161-2171